Hydrodynamics of non-equilibrium soil water retention

Itai Einav[1], Mario Liu[2]

[1]Sydney Centre in Geomechanics and Mining Materials, School of Civil Engineering, The University of
Sydney, 2006, Sydney, Australia
[2]Theoretische Physik, Universität Tübingen, 72076 Tübingen, Germany

Key Points:

- A thoroughly rigorous hydrodynamic theory for partially saturated soil is developed that distinguishes metastable from true equilibrium states
- Departure from true equilibrium is controlled by a granular temperature that signifies mesoscopic motions of particle and fluid interfaces
- The theory explains the rich complexity of soil water retention, including hydraulic hysteresis, path-dependent air entrapment and negative suction

Corresponding author: Itai Einav, `itai.einav@sydney.edu.au`

Abstract

Water retention in soil exhibits diverse phenomena, including suction-saturation hysteresis, non-unique air entrapment at zero suction and negative suction under partial saturations. The constancy of suction after a long rest can be broken by relatively minor mechanical or hydraulic agitations such as low-amplitude wetting cycles – this fact is here being related to metastable states that differ from the true equilibrium. The complete suction-saturation relationships are thus being recovered using non-equilibrium Landau's hydrodynamic theory and Onsager's reciprocity principles. Equilibrium suction does not pertain to hysteresis, yet can be approached through small amplitude agitations over long duration. Conditions for rate independence are being described, while rate-dependency are also accommodated and illustrated. Finally, it is shown that the new non-equilibrium theory retains the rigorously derived equilibrium result of the effective stress of partially saturated soils.

1 Introduction

The connection of air and water pressures to their densities in partially saturated soils is normally expressed by relating suction (air minus water pressures) to the degree of saturation and porosity. These soil water retention relationships, which are known alternatively as capillary pressure-saturation relations, are critical to hydrology, agriculture, geotechnology and petroleum engineering, as they control transport phenomena (Bear, 2013; Hassanizadeh et al., 2002) and effective stresses (Jiang et al., 2017; Vaunat & Casini, 2017). From previous experimental research of these relationships many phenomena have been identified. Most generally, under elevated suctions the amount of water in the soil reduces (Brooks, 1965; Mualem, 1976), while under constant suction the degree of saturation depends on the porosity (Gallipoli et al., 2003; Assouline, 2006; Zhou et al., 2012). Drying from full saturation occasionally requires large suction to distinguishably reduce the water content or saturation (Fredlund & Xing, 1994; Pasha et al., 2017). Wetting monotonously from dry states cannot regain full saturation without entrapping air and letting water pressure gets larger than the air pressure, meaning essentially negative suction or capillary pressure (Skjaeveland et al., 2000; Alsherif et al., 2015; Wang et al., 2016; Chen et al., 2019). Under zero suction the degree of saturation is also not unique and broadly depends on the maxima of previously applied suction (Poulovassilis, 1970; Wardlaw & Taylor, 1976; Hammervold et al., 1998). Cycles of wetting (imbibition) and drying (drainage) present hysteretic (scanning) response (Haines, 1930; Gallipoli, 2012; Zhou, 2013; Pasha et al., 2017). While the effective stress of soils has been fundamentally linked to soil water retention under thermodynamic equilibrium conditions (Jiang et al., 2017), for all practical purposes the impact of hydraulic hysteresis on it seems negligible when experimentally plotted against saturation (Khalili & Zargarbashi, 2010).

In the well-known work of (Hassanizadeh & Gray, 1993) thermodynamics were used to articulate a number of useful restrictions on soil water retention (*viz.*, capillary pressure-saturation) relationships. However, there is currently no thermodynamic framework capable of explaining all the above listed observations using a single mathematically consistent physical treatment – the purpose of this paper is to resolve this gap by extending a previous formulation for thermodynamically equilibrated soil systems (Jiang et al., 2017; Einav & Liu, 2018, 2020) to non-equilibrium conditions. In particular, here the phenomena of hydraulic hysteresis, air entrapment, path-dependent saturation at zero suction and negative suction will all be resolved using a single evolution equation for suction deviation from a well defined non-hysteretic true equilibrium retention state, without needing to take any additional assumptions.

The current derivation follows the *hydrodynamic procedure*, which was originally formulated by Landau (Landau & Lifshitz, 1980, 1987), and extended to address super fluidity (Khalatnikov, 2018) and liquid crystals (de Gennes & Prost, 1993). More recently

the concept of two-stage irreversibly in heterogeneous media was introduced by (Jiang & Liu, 2009), and adopted for granular materials (Jiang & Liu, 2009, 2015; Alaei et al., 2021). Similarly, (Jiang et al., 2017) have hydrodynamically derived the effective stress of partially saturated soils in thermodynamic equilibrium, without needing to track the overwhelmingly complex shapes and distribution of air-water-solid interfaces, thanks to the fact that all these factors are actually encoded in the soil water retention relations. Here, their resolved relationship between the effective stress and soil water retention is shown to be valid even under non-equilibrium conditions.

To accommodate for non-equilibrium relations between fluid pressures and densities, the current treatment adopts the Onsager's reciprocity relations (Onsager, 1931; De Groot & Mazur, 2013) for the corresponding dissipative microscopic processes. The relevance of these relations has been noted for porous media by (Bear, 2013) and others (Li et al., 1995; Moyne & Murad, 2006; Winkler et al., 2020), though have not been used to explain hysteretic soil water retention in soil. Furthermore, unlike the earlier thermodynamic formulations of partially saturated soils, we do not neglect the subtle yet rigorous distinction (Jiang et al., 2017) between the externally applied or measured suction and the intrinsic suction that actually develops in the media. Those could be an order magnitude different, yet they are strictly connected thermodynamically.

Another key step in the current hydrodynamic derivation is the inclusion of more than one set of temperatures and entropies. Although in water research only the thermal temperature has been considered prior to this work, additional temperatures have been accounted for in continuum formulations of granular and amorphous materials (Jiang & Liu, 2009; Kamrin & Bouchbinder, 2014). Here we adopt the two stage irreversibly principle for energy flow between temperatures of distinct scales of motion (Jiang & Liu, 2009), and identify two sets of temperatures and entropies. The first set includes the conventional thermal temperature and entropy (T and s), which captures the degrees of freedom and fluctuating motion of elementary atomistic particles. The second set includes the meso-related temperature and entropy (T_m and s_m), which embodies the degrees of freedom and fluctuating motion of mesoscopic features at the scale of soil particles and the water-air-particle interfaces in between. The scales of these mesoscopic features are comparable and overwhelmingly larger than that of atoms, and thus their contributions are lumped within the single set of T_m and s_m.

Thermal effects on soil water retention have been reported experimentally (Hopmans & Dane, 1986). These could be naturally accounted for in the theory, but are left for future considerations since they tend to be small in practical regimes of interest. On the other hand, the dependence of soil water retention on the fluctuating motion of soil particles and fluid-solid interfaces has not been considered (*eg.*, through T_m) in previous thermodynamic considerations; here, this concept is being developed, thus allowing to capture relaxation towards the least energy states of true equilibrium (see Fig 1a).

The significance of the 'true equilibrium' for soil water retention relationships is clearly demonstrated, and the corresponding states are shown to be unique for every given material. This is in contrast to the previous thermodynamic ideas by (Morrow, 1970) and (Hassanizadeh & Gray, 1993), which involved two different equilibrium relationships for drying and wetting. However, such models fail to decide where to relax to when residing in between, unless being forced to arbitrarily (Beliaev & Hassanizadeh, 2001). As such the previous models cannot explain why the soil can develop negative suction (or negative capillary pressures). Similarly, they cannot explain the non-uniqueness of residual saturation, air entrapment, and the approach of suction towards a focal point upon wetting-drying cycles with diminishing amplitude (Muraleetharan et al., 2009).

In contrast, the current formulation is shown to predict all of these observations from first principles. At non-equilibrium conditions, the retention state tends to get stuck only at shallow energy minima. These minima are rather precarious, because they could
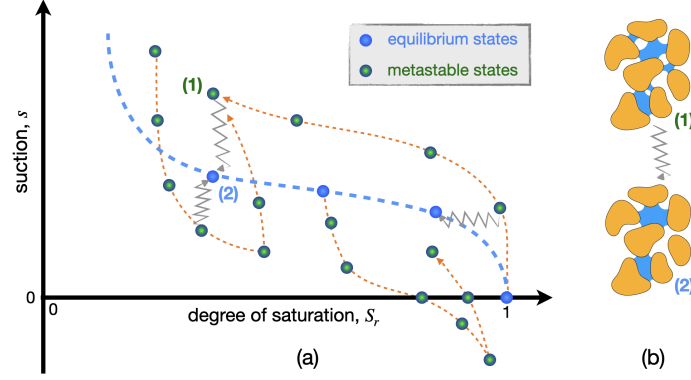
Figure 1: Conceptual distinction between equilibrium and metastability: (a) soil water retention showing metastable states visited after monotonic drying or wetting (dashed orange lines) and true equilibrium states (dashed blue line) approached after low amplitude perturbations of suction or saturation (grey zigzags), or even acoustic waves; (b) the dynamics of fluid patches and interfaces that accompany such perturbations.

be easily left behind upon small hydraulic or mechanical vibrations. The states belonging to these minima are only *metastable* and are not actually in equilibrium (see Fig 1a). On the other hand, by continuously adding further hydraulic or mechanical vibrations to the soil, the state can gradually approach the true equilibrium state of least energy, because micromechanically this can unlock the motion of otherwise feebly jammed fluid patches (see Fig 1b). Experiments that impose such vibrations at both positive (Muraleetharan et al., 2009) and negative (Alsherif et al., 2015) suctions are available in the literature, and support the presence of only a single true equilibrium state.

Partially saturated soils are three-phase media, where each phase interacts with the others. According to the proposed theory, small solid particle vibrations (for example, excited by acoustic waves) would cause the meso-related temperature T_m to elevate. Increased value of T_m means stronger motion of localised fluid patches. In the process these patches migrate to explore other locations in the pore spaces, where they could more favourably rest. This motion is accompanied by the alterations of interfacial fluid-particle geometries (see Fig 1b), and thus changes to the measured suction. As the mechanical agitation stops and T_m relaxes back to zero, the system attain a new metastable state of suction, which may possibly lie on the true equilibrium curve (see Fig 1a), without even needing to experience any change to the degree of saturation S_r. This simple thought experiment illustrates why particle motion should not be disconnected from soil water retention. The proposed hydrodynamic theory considers this form of coupling for the first time, as well as recovering the other form of solid-fluid coupling between effective stress and fluid pressures in soils.

The paper is organised as follows. In Sec. 2 the hydrodynamic principles for partially saturated soils will be reviewed, being valid for both equilibrium and non-equilibrium conditions. Based on these general principles, the following Sec. 3 summarises the previously derived specific results of partially saturated soils under thermodynamic equilibrium; the presentation will add new context and examples to support the remaining, main parts of the paper. In the following sections the formulation will be extended to non-equilibrium conditions. In Sec. 4 the treatment will focus on rate-independent processes; while Sec. 5 will expand this formulation to rate-dependent processes which in the limit of slow drying and wetting predicts similar results as along the rate-independent limit in Sec. 4. Both of these sections will include a number of examples to illustrate the

significance of the new theory. Finally, in the concluding Sec. 6 the novel concepts of this paper will be summarised, followed by a number of suggestions for future considerations and studies.

2 General hydrodynamics for partially saturated soils

2.1 Densities

Partially saturated soils contain three domains denoted by an index $\beta = \{S,W,A\}$, each species sufficiently dispersed such that it could be statistically macroscopic for thermodynamics to hold in it. The soil has a representative volume V where each species has a mass M_β; as a result, three thermodynamic partial densities can be identified, whose addition gives the overall partial density:

$$\varrho_\beta \equiv \frac{M_\beta}{V}, \ \varrho \equiv \sum \varrho_\beta. \tag{1}$$

Similarly, it is possible to define corresponding intrinsic densities using the species volumes V_β, which add up to give the total volume:

$$\hat{\varrho}_\beta \equiv \frac{M_\beta}{V_\beta}, \ V \equiv \sum V_\beta. \tag{2}$$

Using these densities a variety of commonly used dimensionless ratios could be defined:

$$c_\beta \equiv \frac{M_\beta}{M} = \frac{\varrho_\beta}{\varrho}, \quad \phi_\beta \equiv \frac{V_\beta}{V} = \frac{\varrho_\beta}{\hat{\varrho}_\beta},$$
$$n \equiv \frac{V_V}{V} = \phi_W + \phi_A, \quad e \equiv \frac{V_V}{V_S} = \frac{n}{1-n}, \quad S_r \equiv \frac{V_W}{V_V} = \frac{\phi_W}{n}, \tag{3}$$

being the concentrations and volume fractions of the species, the porosity, void ratio, and the degree of saturation, respectively; while $V_V = V_A + V_W$ is the volume of voids. The key point here is that all the above ratios are entirely given from the six densities (three partials and three intrinsics).

Finally, using simple additions

$$\sum \phi_\beta \equiv 1, \quad \sum c_\beta = 1. \tag{4}$$

2.2 Balance laws

According to the first law of thermodynamics all media must conserve energy, which is given by the balance of the conserved energy density (U):

$$\partial_t U + \nabla_i E_i = \varrho v_i G_i, \tag{5}$$

where E_i is the energy flux, ϱG_i is the gravitational force density, and v_i is the barycentric velocity. The conserved energy is related to its value at rest ($v_i = 0$), known as the internal energy density (u):

$$U \equiv U(g_i, \jmath, \varepsilon_{ij}^e, \varrho_\beta, N_\zeta) = g_i^2/(2\varrho) + u(\jmath, \varepsilon_{ij}^e, \varrho_\beta, N_\zeta), \tag{6}$$

where $g_i = \varrho v_i$, $\jmath$, ε_{ij}^e and ϱ_β represent the momentum, thermal entropy, the elastic strain tensor, and the partial densities of the three β-species in Eq. (1), respectively. These state variables are universally required for the description of partially saturated soils under both equilibrium and non-equilibrium conditions. On the other hand, the term N_ζ denotes a list of ζ later-to-be-specified non-equilibrium state variables, whose values vanish under equilibrium. All these equilibrium and non-equilibrium state variables require

their own balance law. Below, these evolution laws are specified for the equilibrium variables, leaving the non-equilibrium variables for Sec. 4.

The momentum density is given by its own conservation law:

$$\partial_t g_i + \nabla_j (g_i v_j + \sigma_{ij}) = \varrho G_i, \tag{7}$$

where σ_{ij} is the total stress tensor.

The thermal entropy is given from the second law of thermodynamics:

$$\partial_t s + \nabla_i (s v_i - F_i) = R/T \geq 0, \tag{8}$$

where $s v_i$ and F_i are the convective and dissipative energy currents, respectively; while R and T are the thermal entropy production and temperature.

The elastic strain tensor is given from:

$$d_t \varepsilon_{ij}^e + \Omega_{ik} \varepsilon_{kl}^e - \varepsilon_{kj}^e \Omega_{ik} = \dot{\varepsilon}_{ij} - \dot{\varepsilon}_{ij}^p, \quad d_t = \partial_t + v_k \nabla_k, \tag{9}$$

where Ω_{ij} is the anti-symmetric component of the velocity gradient, $\dot{\varepsilon}_{ij} = -\frac{1}{2}(\nabla_i v_j + \nabla_j v_i)$ the total symmetric strain rate, while $\dot{\varepsilon}_{ij}^p$ is its dissipative current known as the plastic strain rate. More detail on the significance of this law is given by (Einav & Liu, 2018).

Finally, the balance law for the partial densities of the three species, as well as the overall conservation law for the total partial density are given from:

$$\partial_t \varrho_\beta \equiv -\nabla_i (\varrho_\beta v_i^\beta) = -\nabla_i (\varrho_\beta v_i - J_i^\beta), \quad \partial_t \varrho \equiv -\nabla_i (\varrho v_i), \tag{10}$$

where v_i^β and J_i^β are the velocity and dissipative density current (flux) of species β. In particular, the sum of the species momenta is given by the total momentum density of the soil mixture

$$\varrho v_i = \sum \varrho_\beta v_i^\beta, \tag{11}$$

while thanks to Eq. (1) we also find $\partial_t \varrho = \sum \partial_t \varrho_\beta$, so by combining the above:

$$\sum J_i^\beta = 0 \quad \Rightarrow \quad J_i^\beta = \varrho_\beta (v_i - v_i^\beta). \tag{12}$$

2.3 Hydrodynamic procedure – general results

Following the hydrodynamic procedure (Einav & Liu, 2018), by combining Eqs. (6-12) the thermal temperature is recovered from its corresponding entropy density:

$$T \equiv \frac{\partial u}{\partial s}, \tag{13}$$

while the elastic stress, thermodynamic pressure, and viscous stress are given by:

$$\sigma_{ij}^e \equiv \frac{\partial u}{\partial \varepsilon_{ij}^e}, \quad P_T \equiv -\frac{\partial (u/\varrho)}{\partial (1/\varrho)}\bigg|_{\varepsilon_{ij}^e}, \quad \sigma_{ij}^D = \sigma_{ij} - \sigma_{ij}^e - P_T \delta_{ij}, \tag{14}$$

where δ_{ij} is the Kronecker delta tensor. Similarly, it is possible to define a variety of partial chemical potentials for the total mixture, individual species, and for their deviation from the chemical potential of the solid phase:

$$\mu \equiv \frac{\partial u}{\partial \varrho}, \quad \mu_\beta \equiv \frac{\partial u}{\partial \varrho_\beta}, \quad X_\beta \equiv \mu_\beta - \mu_S. \tag{15}$$

Thanks to the hydrodynamic procedure (Einav & Liu, 2018) it is also possible to derive the rate of thermal entropy production:

$$R = F_i \nabla_i T_m + J_i^A \nabla_i X_A + J_i^W \nabla_i X_W + \mathcal{D} \geq 0, \quad \mathcal{D} = \sigma_{ij}^D \dot{\varepsilon}_{ij} + \sigma_{ij}^e \dot{\varepsilon}_{ij}^p, \tag{16}$$

174   where $\mathcal{D}$ is identified as the mechanical dissipation.

While the general condition for guaranteeing the positiveness of the thermal entropy production R may follow from Onsager's reciprocal relationships, to a first order it is clear that $\sigma_{ij}^{\mathrm{D}} \sim \dot{\varepsilon}_{ij}$. Critical state testing in soil mechanics are generally made under very low strain rates, in which case the viscous stress practically vanishes $\sigma_{ij}^{\mathrm{D}} \to 0$. So by identifying the elastic stress as effective (as both comes to represent the stress carried out only by the soil skeleton), the hydrodynamic procedure reveals the following general result for the effective stress of soils (both fully saturated and not):

$$\sigma_{ij}^{\mathrm{eff}} \equiv \sigma_{ij} - P_T \delta_{ij}, \quad P_T = -\frac{\partial(u/\varrho)}{\partial(1/\varrho)} = \mu\varrho - u. \tag{17}$$

175   Since P_T depends on the definition of u, so does the explicit solution for the effec-
176 tive stress $\sigma_{ij}^{\mathrm{eff}}$. Importantly, as discussed in the following section the general dependence
177 of u on the various densities is clear, thus enabling accurate solutions for both P_T and
178 $\sigma_{ij}^{\mathrm{eff}}$.

179 **3 Partially saturated soils under equilibrium**

180   The current section reviews the fundamental results from the thermodynamic deriva-
181 tion for equilibrated soil systems by (Jiang et al., 2017), which reveals the explicit hy-
182 dromechanical relationships between the effective stress of partially saturated soils to their
183 intrinsic and externally measured/applied suction values. This is an essential step be-
184 fore proceeding to address the more general case of such relationships under non-equilibrium
185 conditions.

186 **3.1 Equilibrium conditions**

True thermodynamic *equilibrium* states refer to conditions where all the dissipative fluxes in the system vanish and all the non-equilibrium state variables attain zero value, so that their contribution to the energy vanishes. Under such conditions the internal energy u approaches its unique minimum value:

$$\min_{\{\hat{\varrho}_\beta, N_\zeta\}} u(s, \varepsilon_{ij}^{\mathrm{e}}, \varrho_\beta, \hat{\varrho}_\beta, N_\zeta) = u_{\mathrm{eq}}(s, \varepsilon_{ij}^{\mathrm{e}}, \varrho_\beta) \quad \text{[equilibrium]} \tag{18}$$

187 which is found by minimising the internal energy over the three intrinsic densities $\hat{\varrho}_\beta$ (Jiang
188 et al., 2017), as well as all the possible values of the yet-to-be-specified ζ non-equilibrium
189 state variables N_ζ. In the following, this equilibrium state is first described by specify-
190 ing u_{eq}, and later $\zeta = 2$ specific non-equilibrium state variables will be defined to al-
191 low departures from the true equilibrium conditions. At non-equilibrium conditions, it
192 would be shown using the new theory that partially saturated soils could get stuck in
193 metastable states that do not satisfy the true equilibrium condition of least energy.

194 **3.2 Internal energy**

Neglecting thermal effects through s (or T) on the hydromechanical relations, the equilibrium value of the internal energy of partially saturated soils could be represented by summing up the elastic strain energy of the soil skeleton u_{e} and the free energy f of the three domains:

$$u_{\mathrm{eq}} \equiv u_{\mathrm{e}}(\varepsilon_{ij}^{\mathrm{e}}, \varrho_{\mathrm{S}}) + f(\varrho_\beta). \tag{19}$$

The relation between the partial densities in Eq. (1) means that f varies with ϱ. Therefore, since u_{e} and f depend on ϱ they both contribute to the thermodynamic pressure P_T. However, wave measurements reveal elastic bulk moduli in soil at the order $\sim (\varrho_{\mathrm{S}}^3 p^{\mathrm{e}})^{1/2}$ (Rubin & Einav, 2011; Viggiani & Atkinson, 1995), meaning elastic pressure

$p^{\mathrm{e}} \sim \varrho_{\mathrm{S}}^3 (\varepsilon_v^{\mathrm{e}})^2$ and elastic energy $u_{\mathrm{e}} \sim \varrho_{\mathrm{S}}^3 (\varepsilon_v^{\mathrm{e}})^3$ (where $p^{\mathrm{e}} = \frac{1}{3}\sigma_{ii}^{\mathrm{e}}$ and $\varepsilon_v^{\mathrm{e}} = \varepsilon_{ii}^{\mathrm{e}}$). Thus, although it is possible to carry along the contribution of u_{e} to P_T through its own dependence on ϱ within ϱ_{S}, this is entirely negligible relative to the contribution of f since most practically $\varepsilon_v^{\mathrm{e}} \lesssim 0.1$. Therefore, it is accurate to replace u by f in both Eq. (17) and Eqs. (14,15,13) so that:

$$\sigma_{ij}^{\mathrm{eff}} \equiv \sigma_{ij} - P_T \delta_{ij}, \quad P_T = -\frac{\partial(f/\varrho)}{\partial(1/\varrho)} = \mu\varrho - f, \tag{20}$$

and

$$\sigma_{ij}^{\mathrm{e}} = \frac{\partial u_{\mathrm{e}}}{\partial \varepsilon_{ij}^{\mathrm{e}}}, \quad \mu = \frac{\partial f}{\partial \varrho}, \quad \mu_\beta = \frac{\partial f}{\partial \varrho_\beta}, \tag{21}$$

respectively. As shown below, the dependence of f on the various densities is clear, thus enabling an accurate solution for P_T and $\sigma_{ij}^{\mathrm{eff}}$.

3.3 Free energy and suctions

The free energy of the three domains, which represents their volumetric compressibility, could be calculated analytically (Jiang et al., 2017):

$$f \equiv \sum \phi_\beta \hat{f}_\beta(\hat{\varrho}_\beta) = \sum \frac{\varrho_\beta}{\hat{\varrho}_\beta} \hat{f}_\beta(\hat{\varrho}_\beta), \quad \hat{P}_\beta \equiv -\frac{\partial(\hat{f}_\beta/\hat{\varrho}_\beta)}{\partial(1/\hat{\varrho}_\beta)} = \hat{\mu}_\beta \hat{\varrho}_\beta - f_\beta, \quad \hat{\mu}_\beta \equiv \frac{\partial \hat{f}_\beta}{\partial \hat{\varrho}_\beta}, \tag{22}$$

where $\hat{f}_\beta$, $\hat{P}_\beta$ and $\hat{\mu}_\beta$ are the intrinsic free energy, pressure and chemical potential of species β arising due to possible small variations in the corresponding intrinsic densities $\hat{\varrho}_\beta$. Although small relative to variations in partial densities ϱ_β, the possibility of variable $\hat{\varrho}_\beta$ must be allowed for to accomodate phenomena related to the development of air-water-solid interfaces under partial saturations. In particular, under partial saturations such variations produce different signs for the intrinsic pressures in the air and the water, thus producing intrinsic suction:

$$\hat{s} \equiv \hat{P}_{\mathrm{A}} - \hat{P}_{\mathrm{W}}, \tag{23}$$

which should not be confused with the measured suction from the difference between the air (u_{A}) and water (u_{W}) pressures that are being applied or measured externally from devices out of the soil:

$$s \equiv u_{\mathrm{A}} - u_{\mathrm{W}}. \tag{24}$$

Although not being considered prior to (Jiang et al., 2017), most usually $u_{\mathrm{A}} \neq \hat{P}_{\mathrm{A}}$, $u_{\mathrm{W}} \neq \hat{P}_{\mathrm{W}}$, and $s \neq \hat{s}$, since along boundaries only the partial chemical potentials in and out of the measurement devices need to be equal under equilibrium.

Furthermore, while under equilibrium the presence of surface tensions along the geometrically complicated interfaces means water decompression ($\hat{P}_{\mathrm{W}} < 0$, $u_{\mathrm{W}} < 0$), compressed air pressures ($\hat{P}_{\mathrm{A}} > 0$, $u_{\mathrm{A}} > 0$), and thus positive suctions ($\hat{s} > 0$, $s > 0$), it will be shown later that off equilibrium these suctions could change sign upon wetting from very dry samples.

3.4 Energy minimisation, and equilibrium suctions and effective stress

As presently stated in Eq. (22a) the free energy f depends on six densities – the three partial ones required for Eq. (19), as well as three non-required intrinsic densities $\hat{\varrho}_\beta$. Therefore, solving for the effective stress in Eq. (20) would depend on too many intrinsic densities. To this end it is possible to first solve equilibrium states by minimising the energy towards its global minimum (Jiang et al., 2017), before addressing non-equilibrium scenarios where the states can get stuck in local minima.

As part of the energy minimisation, it is understood that under a given set of partial densities ϱ_β, the intrinsic densities $\hat{\varrho}_\beta$ would adjust dependently to minimise the energy. When the energy is minimised, while taking Eq. (4) as the only trivial constraints,

one finds $P_T = \hat{P}_\beta = u_\beta = P_0$ as a suctionless limit where $\hat{s} = s = 0$. However, such a trivial solution ignores the previously mentioned role of interfacial phenomena in partially saturated soil, as the actual reason for observing the non-zero measured and intrinsic suctions in the first place. Previous attempts to track the complex geometries of such interfaces in soils have always relied on oversimplifying assumptions. As detailed by (Jiang et al., 2017) a more pragmatic, accurate and general approach is to consider the measured suction s as an actually known quantity by minimising the energy with the intrinsic suction $\hat{s}$ as an additional constraint. This actually has an exact analytic solution, but the solution is far too long to be illuminating. However, it is possible to arrive at practically the same result as the analytic one by approximating it around the suctionless limit (Jiang et al., 2017), which presents the following structure for equilibrium states

$$P_T \equiv u_A - \chi s, \quad \chi \equiv \chi(\varrho_\beta), \tag{25}$$

213   where χ is the classical Bishop's coefficient (Bishop & Blight, 1963).

Further keeping in mind the order of magnitudes of both the compressibilities K_β and intrinsic densities $\hat{\varrho}_\beta$ of the three species, with air by far having the smallest, thus negligible values, we find that under equilibrium conditions:

$$\chi_{\rm eq} \equiv \chi_{\rm eq}(\varrho_\beta) = \frac{\varrho_A}{\bar{\varrho}_A} + \frac{\varrho_S}{\bar{\varrho}_S}\left[\frac{\bar{\varrho}_A(\partial\hat{s}_{\rm eq}/\partial\varrho_A) - \bar{\varrho}_S(\partial\hat{s}_{\rm eq}/\partial\varrho_S)}{\bar{\varrho}_A(\partial\hat{s}_{\rm eq}/\partial\varrho_A) - \bar{\varrho}_W(\partial\hat{s}_{\rm eq}/\partial\varrho_W)}\right], \tag{26}$$

$$s_{\rm eq} \equiv s_{\rm eq}(\varrho_\beta) = \frac{\varrho_W}{\bar{\varrho}_W K_W}\left[\bar{\varrho}_A\frac{\partial\hat{s}_{\rm eq}}{\partial\varrho_A} - \bar{\varrho}_W\frac{\partial\hat{s}_{\rm eq}}{\partial\varrho_W}\right]\hat{s}_{\rm eq}, \tag{27}$$

214   where the subscript 'eq' was added to χ, s and $\hat{s}$ to highlight that the above solutions
215   correspond to equilibrium values, owing to the energy minimisation. The purpose of adding
216   this now as compared to the original exposition (Jiang et al., 2017) is that in the follow-
217   ing equilibrium would be distinguished from non-equilibrium conditions. Furthermore,
218   while as part of the energy minimisation the intrinsic densities $\hat{\varrho}_\beta$ were allowed to vary
219   to obtain the above result, these variations are certainly small and thus their assigned
220   value in the above could be their reference value $\bar{\varrho}_\beta$ under room temperature and atmo-
221   spheric air pressure. It is also noted that the water compressibility at those conditions
222   is known to be $K_W = 2$ GPa.

223   The relationships in Eqs. (26,27) are most general and accurate, and simply require
224   one to assume a dependence in the form $\hat{s}_{\rm eq} = \hat{s}_{\rm eq}(\varrho_\beta)$ to yield measured soil water re-
225   tention in the form $s = s(\varrho_\beta)$ that could be compared with experimental measurements.
226   Although the intrinsic densities were allowed to change during the energy minimisation
227   to arrive to the results above, these changes are entirely small and thus rather than the
228   generally variable $\hat{\varrho}_\beta$ we have used $\bar{\varrho}_\beta$ above as constant intrinsic densities that corre-
229   spond to their known values at 1 atm and room temperature.

Although in general the effects of the intrinsic air density on the hydromechanics of soils is considered in the above, most empirical soil water retention relationships tend to neglect this theoretical contribution. It is thus useful to neglect the effects of $\hat{\varrho}_A$ in the above, and further consider the relationships between the index properties in Eq. (3) to produce more common dependencies and simpler structures. One such possibility can be exhibited in terms of the degree of saturation S_r and void ratio e (Einav & Liu, 2020):

$$\chi_{\rm eq} \equiv \chi_{\rm eq}(S_r, e) = S_r - e\frac{\partial\hat{s}_{\rm eq}/\partial e}{\partial\hat{s}_{\rm eq}/\partial S_r}, \tag{28}$$

$$s_{\rm eq} \equiv s_{\rm eq}(S_r, e) = -\left[\frac{S_r}{K_W}\frac{\partial\hat{s}_{\rm eq}}{\partial S_r}\right]\hat{s}_{\rm eq}, \tag{29}$$

230   which requires one to assume $\hat{s}_{\rm eq} = \hat{s}_{\rm eq}(S_r, e)$ that would yield measured soil water re-
231   tention in the form $s = s(S_r, e)$ agreeable with the experiments.

3.5 Illustration of equilibrium states

The analytic way to use the relationships in Eqs. (28,29) is to treat Eq. (29) as an ordinary differential equation (ODE), to be solved for $\hat{s}_{\text{eq}}$. Given a known empirical law for $s_{\text{eq}} = s_{\text{eq}}(S_r, e)$, it is possible to integrate this ODE to get $\hat{s}_{\text{eq}} = \hat{s}_{\text{eq}}(S_r, e)$ using an initial suctionless boundary at full saturation $\hat{s}(1, e) \equiv 0$. One example for such analytic solutions is to impose a hyperbolic relationship between suction and saturation (Jiang et al., 2017; Einav & Liu, 2018, 2020). An alternative example is developed through the two steps below, which yield relationships whose mathematical forms appear somewhat more versatile and elegant than the previously proposed hyperbolic relations.

(a) As a first step, consider retention functions inspired by a three-parameter (c, α, λ) Inverse Weibull function. Where this function was originally used to estimate distributed strength in solid materials, here it is adapted to represent the dependence of suction on saturation:

$$s_{\text{eq}} = ce^{-\lambda}(-\ln S_r)^\alpha, \tag{30}$$

where α is a constant controlling the dependence of soil water retention curves on S_r; while $ce^{-\lambda}$ controls its dependence on void ratio (which could be estimated from empirical relations for air entry values). Putting this proposition in Eq. (29) and solving using $\hat{s}(1, e) \equiv 0$ as boundary condition, we find:

$$\hat{s}_{\text{eq}} = \sqrt{\tfrac{2K_{\text{W}}}{1+\alpha}(-\ln S_r)s_{\text{eq}}}. \tag{31}$$

which upon differentiation using Eq. (28) gives:

$$\chi_{\text{eq}} = S_r\left(1 + \tfrac{\lambda}{1+\alpha}\ln S_r\right). \tag{32}$$

(b) While the suctions in the proposed relations above diverge at zero saturations, some soils exhibit diverging behaviour at a finite small value of residual saturation S_{r0} (as an additional fourth parameter). To that extent, it is possible to extend the above relations by first replacing S_r in $\hat{s}_{\text{eq}}$ from Eq. (31) with an effective saturation $S_r^* = (S_r - S_{r0})/(1 - S_{r0})$, so that from Eqs. (28,29):

$$s_{\text{eq}} = ce^{-\lambda}\left(\tfrac{S_r}{S_r - S_{r0}}\right)(-\ln S_r^*)^\alpha, \tag{33}$$

$$\hat{s}_{\text{eq}} = \sqrt{\tfrac{2K_{\text{W}}}{1+\alpha}(-\ln S_r^*)s_{\text{eq}}}. \tag{34}$$

$$\chi_{\text{eq}} = S_r\left(1 + \tfrac{\lambda(S_r - S_{r0})}{(1+\alpha)S_r}\ln S_r^*\right), \tag{35}$$

which yields the same results for $S_{r0} = 0$ as with Eqs. (30-32).

To illustrate these functions, Fig. 2 shows the dependence of the intrinsic and measured suctions on the shape parameter α. The results have been non-dimensionalised to exclude the effects of the void ratio e and parameter λ, which do not change the qualitative shape and merely scale the value of the effective air entry value in this model (the effective air entry value represents the required suction to start drying the sample from full saturation). Nevertheless, the parameter λ alters the result for the effective stress Bishop's coefficient χ_{eq}, as shown for $\lambda = 1$ and $\lambda = -1$ on Fig. 3a and Fig. 3b, respectively, for various values of α. Both α and λ affect the qualitative dependence of χ_{eq} on S_r.

Comparing Fig. 2a and Fig. 2b, it is clear that the equilibrium intrinsic and measured suctions are not similar both qualitatively and in values (since the normalisation differ), as discussed by (Einav & Liu, 2020). In Fig. 2 an increase in α is shown to produce a sharper rise at high saturations followed by a flatter rise at intermediate saturations, transitioning from typical clay to typical sand retention curves. This effect is
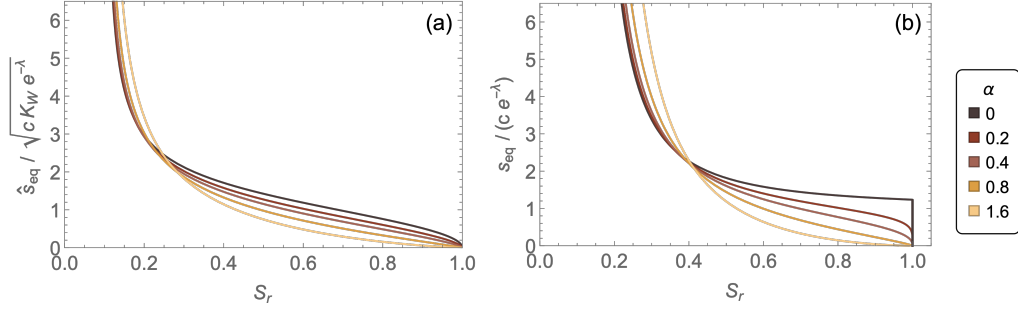
Figure 2: The dependence under the true thermodynamic equilibrium of the (a) intrinsic and the (b) measured suctions on the degree of saturation for different retention shape parameter α using Eqs. (34,33), respectively. These suctions have been normalised to yield non-dimensional numbers on the y-axes. The residual saturation parameter $S_{\mathrm{r}0} = 0.1$
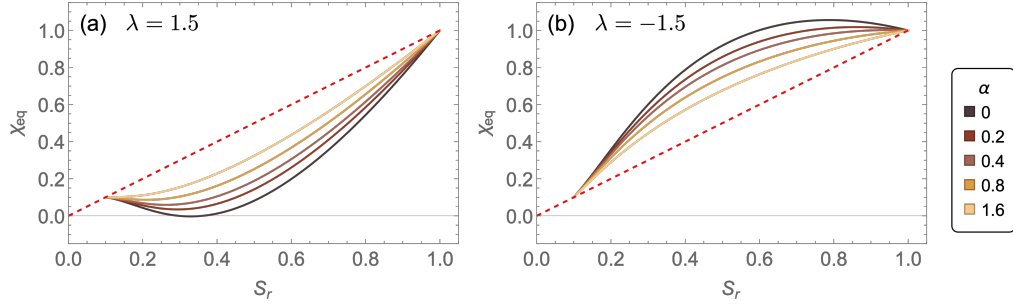

Figure 3: The dependence of the Bishop parameter $\chi = \chi_{\mathrm{eq}}$ on the degree of saturation S_r for different shape parameter α and (a) positive $\lambda = 1.5$ or (b) negative $\lambda = -1.5$, corresponding to Eq. (35). As in Fig. 2, the residual saturation parameter $S_{\mathrm{r}0} = 0.1$. Dashed red lines show the trivial $\chi = S_r$ solution, which the current model reproduces with $\lambda = 0$.

particularly clear from the equilibrium measured suction Fig. 2b, where for $\alpha \to 0$ we recover a true air entry value signal at $S_r = 1$. On the other hand Fig. 3a,b illustrate that positive and negative λ values yield χ_{eq} values below and above the $\chi_{\mathrm{eq}} = S_r$ line, respectively. Both scenarios have been reported in the literature (Jennings & Burland, 1962; Khalili & Zargarbashi, 2010), showing χ_{eq} values above 1 at high saturations, and hinting towards values that may go below 0 as long as the soil remains stable.

It should also be mentioned that in such measurements of χ (Jennings & Burland, 1962; Khalili & Zargarbashi, 2010), the void ratio e is not normally being prevented from changing during the tests. Such potential e-changes were not included in drawing Fig. 3, which took e to be constant. However, using Eq. (35) the effects of the e variations on the lines could be considered, and would simply distort the $\chi_{\mathrm{eq}} - S_r$ line. The extent of this distortion would depend on the magnitude of the variations of e during the tests and the level of sensitivity of the χ_{eq} relation on it according to Eq. (35).

4 Non-equilibrium soil water retention (rate-independence)

4.1 Non-equilibrium intrinsic suction and effective stress

Under non-equilibrium conditions, the intrinsic and measured suction variables deviate from their equilibrium values, thus exhibiting dynamic phenomena such as hysteresis. It is therefore useful to consider the 'non-equilibrium intrinsic suction' as a new state variable:

$$\xi \equiv \hat{s} - \hat{s}_{\mathrm{eq}}, \tag{36}$$

for which an explicit evolution equation is required. Resolving this equation is the primary focus of the current derivation. To retain the equilibrium results from the previous sections, the evolution of this new independent state variable should obviously relax to zero, so that $\hat{s} \to \hat{s}_{\mathrm{eq}}$ under true equilibrium. Since ξ is independent of all previous state variables (including ϱ_β), then by replacing $\hat{s}_{\mathrm{eq}}$ with $\hat{s}$ in Eqs. (28,29) and using Eq. (36), under non-equilibrium conditions:

$$\chi(\varrho_\beta, \xi) = \chi_{\mathrm{eq}}(\varrho_\beta), \quad s(\varrho_\beta, \xi) = \frac{\hat{s}}{\hat{s}_{\mathrm{eq}}} s_{\mathrm{eq}} = \left(1 + \frac{\xi}{\hat{s}_{\mathrm{eq}}(\varrho_\beta)}\right) s_{\mathrm{eq}}(\varrho_\beta). \tag{37}$$

As such the Bishop stress coefficient χ and thus the thermodynamic pressure in Eq. (25) and the effective stress in Eq. (20) are all insensitive to the non-equilibrium conditions, but the measured suction s is sensitive, since it depends on the value of ξ. This result is valid for any specific exposition, including when the effect of air density on the retention is ignored and the densities are replaced by the saturation and void ratio:

$$\chi(S_r, e, \xi) = \chi_{\mathrm{eq}}(S_r, e), \quad s(S_r, e, \xi) = \left(1 + \frac{\xi}{\hat{s}_{\mathrm{eq}}(S_r, e)}\right) s_{\mathrm{eq}}(S_r, e), \tag{38}$$

where the equilibrium values are taken from Eqs. (28,27), which purely depend on S_r and e.

Since the measured suction depends on the intrinsic suction deviation ξ, one has to track the dynamics of the latter variable. Its general evolution equation should allow it to both advect along the barycentric velocity (v_i) and be dissipated irreversibly through:

$$(\partial_t + v_i \nabla_i)\xi + Z_\xi = 0, \tag{39}$$

where Z_ξ is its dissipative flux. Currently unknown, this dissipative flux will finally be specified by following Onsager's reciprocal conditions and Jiang & Liu's two-stage irreversibility principle (Jiang & Liu, 2009).

4.2 Non-equilibrium, meso-related entropy

In thermodynamics the second law in Eq. (8) refers to balance of thermal entropy in terms of the degrees of freedom of elementary microscopic particles such as atoms. However, the description of soils further requires to consider the degrees of freedom of mesoscopic features such as soil particles and air-water interfacial curvatures, which are many order of magnitudes larger than those atoms. It has been shown and considered that the motion of these mesoscopic features controls the rheology and dynamics of sand. The distributed geometry of air-water interfaces has also been shown experimentally (Zhao et al., 2013; Fukushima et al., 2021) and computationally (Gan et al., 2013) to control soil water retention hysteresis phenomena. Therefore, in addition and in analogy to the balance of the thermal entropy in Eq. (8), we further consider the balance of a meso-related entropy:

$$\partial_t s_{\mathrm{m}} + \nabla_i(s_{\mathrm{m}} v_i - F_i^{\mathrm{m}}) = R_{\mathrm{m}}/T_{\mathrm{m}}, \tag{40}$$

where $s_{\mathrm{m}} v_i$ and F_i^{m} are the meso-related convective and dissipative energy currents, respectively; while R_{m} and T_{m} are the meso-related rates of entropy production and temperature. Here, the above equation lets us consider hydraulically related non-equilibrium

phenomena such as soil water retention hysteresis. However, note that exactly the same equation could and has been used to explain mechanically related non-equilibrium phenomena in sand, such as stress-strain hysteresis (Jiang & Liu, 2009; Alaei et al., 2021). Notice that unlike Eq. (8), R_m is not restricted from being negative, yet we take $R \geq 0$ and $R + R_\mathrm{m} \geq 0$. The micro-meso separation between the two entropies and temperatures has been further discussed by (Liu, 2021) in the context of granular and plasma physics.

4.3 Internal energy at non-equilibrium states

During non-equilibrium conditions the internal energy density of the soil depends on both equilibrium and non-equilibrium contributions, the latter being represented by the two new non-equilibrium state variables, the meso-related entropy $\jmath_\mathrm{m}$ and the intrinsic suction deviation ξ. Therefore, neglecting the effects of the thermal entropy $\jmath$ (or T) on the hydromechanical response of partially saturated soils:

$$u \equiv u(\varrho_\beta, \varepsilon_{ij}^\mathrm{e}, \jmath, \jmath_\mathrm{m}, \xi) = u_\mathrm{eq}(\varepsilon_{ij}^\mathrm{e}, \varrho, \varrho_\beta) + u_\mathrm{ne}(\jmath_\mathrm{m}, \xi), \tag{41}$$

The first term u_eq captures internal energy that maintains during equilibrium and could be taken directly from Eq. (19). On the other hand, the second term u_ne captures additional internal energy at non-equilibrium states. The thermodynamic conjugates of the first three conserved state variables have been defined in Eqs. (21). The thermodynamic conjugates of the two remaining independent state variables are defined from the non-equilibrium part of the internal energy:

$$T_\mathrm{m} = \frac{\partial u_\mathrm{ne}}{\partial \jmath_\mathrm{m}}, \quad Y_\xi = \frac{\partial u_\mathrm{ne}}{\partial \xi}, \tag{42}$$

being the meso-related temperature and 'unbalanced interfacial texture', respectively.

Note that in Eq. (41) the internal energy arising from equilibrium and non-equilibrium state variables was exclusively decoupled into their corresponding contributions. Although this is not necessarily required for the current formulation, this split has been kept for two reasons: (1) there are no current experiments that would support the fine resolution of the accurate form of such coupling; (2) such form of coupling should be expectedly weak, so adding it would only complicate the derivation without changing the actual result of this paper.

Accordingly, since we already specified the equilibrium internal energy in Eq. (19), what is left is to specify the non-equilibrium internal energy in terms of its two non-equilibrium state variables. Again, in the absence of experiments that would help determining its exact form, the simplest form is considered, which involves further decoupling into two independent quadratic contributions from the two non-equilibrium state variables:

$$u_\mathrm{ne}(\jmath_\mathrm{m}, \xi) = \tfrac{1}{2}\omega\jmath_\mathrm{m}^2 + \tfrac{1}{2}\kappa\xi^2, \tag{43}$$

so using Eq. (42):

$$T_\mathrm{m} = \omega\jmath_\mathrm{m}, \quad Y_\xi = \kappa\xi, \tag{44}$$

where $\omega \geq 0$ and $\kappa \geq 0$. The quadratic form of the potential above could be seen as the lowest order term which has a minimum of a Taylor approximation to the otherwise true energy potential. As such, it is clear that as the two new non-equilibrium internal variables vanish ($\jmath_\mathrm{m} \to 0$ and $\xi \to 0$), the total internal energy approaches its minimum equilibrium value $u \to u_\mathrm{eq}$, thus keeping the previous true equilibrium results valid.

Considering again the question of coupling or not the equilibrium and non-equilibrium internal energies in Eq. (41), one may wish to consider the coefficients ω and κ to generally depend on the partial density. However, it could be shown that such generality

would only add an unnecessary negligible contribution to P_T, as illustrated in the context of elasticity in the paragraph that follows Eq. (19). Therefore, taking this option along would not alter the main result of this paper, in the form of the final resolved hydrodynamic equation of non-equilibrium soil water retention.

Combining the non-equilibrium Eqs. (39,40,42) with the previous equilibrium Eqs. (6-12), and following the same hydrodynamic procedure, the total entropy production, which sums up both thermal and meso-related contributions is given by:

$$R + R_m \equiv F_i \nabla_i T + F_i^m \nabla_i T_m + J_i^A \nabla_i X_A + J_i^W \nabla_i X_W + Y_\xi Z_\xi + \mathcal{D} \geq 0. \tag{45}$$

4.4 Total entropy production under typical experimental conditions

The total entropy production in Eq. (45) is most general, being applicable for field and experimental conditions alike. This entropy production is a local quantity, being relevant to any material point in the space, as it depends on both local state variables and gradients. In typical experimental soil water conditions, the only applied gradients come from the fluid fluxes. Under these conditions, we can neglect the thermal and meso-related temperature gradients, as well as the mechanical dissipation, which is mostly driven by negligible velocity gradients. Similarly, it is useful to start by exploring the case of negligible mechanical dissipation, since typical experimental setups for recovering soil water retention properties do not involve discernible mechanical boundary deformations or external acoustic excitation. The impact of such mechanical mechanisms on soil water retention has not been explored experimentally in the literature, but will be detailed theoretically later in Sec. 4.11. Similarly, while fluid fluxes are being imposed in order to determine the soil water retention relationships, the air flux is negligible relative to the water flux, because the density of water is three orders larger than that of air. Accordingly, under experimental conditions we can normally use:

$$\nabla_i T \sim 0, \quad \nabla_i T_m \sim 0, \quad \mathcal{D} \sim 0, \quad J_i^A \ll J_i^W, \tag{46}$$

so that

$$R + R_m = J_i^W \nabla_i X_W + Y_\xi Z_\xi \geq 0. \tag{47}$$

4.5 Parallel force decomposition of the total entropy production

In order to calculate the rates of entropies in Eqs. (8,40) it is necessary to identify the contributions of R and R_m to their cumulative value $R+R_m$ in Eq. (47). Entropy production by $Y_\xi Z_\xi$ effectively arises by departing metastability when interfacial hinges along soil-particle roughness points are unlocked, which vibrate the motion of fluid atoms in the vicinity. Therefore the term $Y_\xi Z_\xi$ is taken to contribute directly and exclusively to the thermal entropy production R, since having it contributing to R_m would not let metastability develop as seen experimentally. On the other hand, we consider two possible decompositions for the $J_i^W \nabla_i X_W$ term: a 'flux decomposition' where the flux term J_i^W is decomposed into atomistic and meso-related parts, and a 'force decomposition' where the chemical force term $\nabla_i X_W$ is broken into two. The use of parallel flux/force decompositions is very common in designing spring-slider systems or electrical circuits. It is also used in hydraulic to calculate effective permeability for porous media with separated solid components. Each of these decomposition formulations has merits, while it is hard to distinguish which of these is more likely without further insight at both scales.

Remarkably, the main result of this paper remains identical at the limit of slow loading using either of these models, yet the force decomposition approach leads to this rate-independent result more directly. Therefore, the parallel force formulation is the one adopted below, while for completeness the alternative parallel flux formulation is given in Appendix A. As part of the alternative formulation a subtle rate-dependence factor arises irrespective of the meso-related temperature T_m, but this does not seem necessary because hydrodynamically speaking rate dependence can always arise from the evolution of T_m as

the physical measure of slowly relaxing fluctuations, as described further in Sec. 5. As far as the mechanical part of the constitutive behaviour is concerned, it is possible to obtain rate-independence even when T_m relaxes, as shown for example for dry sand in terms of the granular temperature (Liu, 2021), which is here considered to contribute to T_m.

Irrespective of these two alternative possible decompositions, it is also noted that the vibration of fluid-solid interfaces should decay to further vibrate the atoms around them. To this extent the R and R_m terms should include source and sink terms ($\pm \gamma T_m^2$), respectively. Accordingly, while the constitutive equations for the various terms will be specified below such that both the total ($R + R_m$) and thermal (R) entropy productions would be strictly non-negative, the meso-related entropy production (R_m) is not restricted from being negative, and here may be so due to the corresponding sink term. This result follows the principle of 'two-stage irreversibility' for the passage of energy from the larger to the smaller scale, which was originally proposed for dry granular materials (Jiang & Liu, 2009), but is here taken to reflect similar hydrodynamics in partially saturated soils.

Taking all of these into account, the overall entropy production is decomposed to its meso-related and thermal contributions, respectively:

$$R_m = J_i^W \nabla_i X_{Wm} - \gamma T_m^2, \tag{48}$$

$$R = J_i^W \nabla_i X_{Wa} + Y_\xi Z_\xi + \gamma T_m^2, \tag{49}$$

where $\nabla_i X_{Wm}$ and $\nabla_i X_{Wa}$ are the meso-related and the thermally-related (atomistic) parts of $\nabla_i X_W$, being the chemical potential gradient of the water relative to the solid. In order to retain Eq. (47) their summation requires:

$$\nabla_i X_{Wa} + \nabla_i X_{Wm} \equiv \nabla_i X_W. \tag{50}$$

The interpretation of the above is that the homogenised fluxes into the sample that goes into moving meso-scopic and atomistic degrees of freedom are equal $J_i^{Wm} = J_i^{Wa} = J_i^W$, yet the forces from the differences in chemical potentials in the two scales are different and add to give the total homogenised potential $\nabla_i X_W$.

4.6 Reciprocal conditions

According to Eqs. (8,47) the non-negativeness of both R and $R + R_m$ must be satisfied. The non-negativeness of the thermal entropy production ($R \geq 0$) is met by adopting Onsager's reciprocal conditions for generally coupled irreversible processes. Accordingly, for the current problem

$$\begin{pmatrix} Z_\xi \\ \nabla_i X_{Wa} \end{pmatrix} = \begin{pmatrix} r^{\xi\xi} & r_j^{\xi W} \\ r_i^{W\xi} & r_{ij}^{WW} \end{pmatrix} \cdot \begin{pmatrix} Y_\xi \\ J_j^W \end{pmatrix}, \tag{51}$$

where we have introduced in the matrix the generalised resistivity coefficients (cofactors of the transport coefficients in (Onsager, 1931)). According to (Casimir, 1945), the resistivity coefficients must satisfy:

$$r_i^{W\xi} = -r_i^{\xi W}, \quad r_{ij}^{WW} = r_{ji}^{WW}, \tag{52}$$

where $r^{\xi\xi} > 0$, $r_{ij}^{WW} > 0$ for $i = j$, and $\det(r_{ij}^{WW}) > 0$.

Furthermore, it is always possible to define

$$r_i^{\xi W} = r^{\xi W} \hat{e}_i, \quad J_i^W = J_W \hat{e}_i, \tag{53}$$

where $r^{W\xi}$ and J_W denote the magnitudes of $r_i^{\xi W}$ and J_i^W, respectively; while $\hat{e}_i$ is taken as the unit vector along which the water flux J_i^W preferentially lies. Then, since $\hat{e}_i\hat{e}_i = 1$, the first Onsager relation in Eq. (51) reduces to:

$$Z_\xi = r^{\xi\xi}Y_\xi + r^{\xi W}J_W. \tag{54}$$

Finally, given the positive diagonal coefficients in Eqs. (51,52) to solve for R in Eq. (49), it is clear that $R \geq 0$. To ensure $R + R_m \geq 0$ we must thus further require

$$\nabla_i X_{Wm} = \eta J_i^W, \tag{55}$$

357   with $\eta \geq 0$.

358   ### 4.7 Water flux through finite experimental volumes

Since $\sum J_i^\beta = 0$ and $J_i^A \ll J_i^W$ from Eqs. (12,46), we also find that $J_i^S \approx -J_i^W$. Using the conservation of solid density in Eq. (10), it follows that its rate of change is $\partial_t \varrho_S = -\nabla_i(\varrho_S v_i + J_i^W)$. However, during experimental water retention tests the solid mass is kept constant ($\partial_t \varrho_S \approx 0$), so we find $J_i^W = -\varrho_S v_i$. Combining the latter relation with the conservation of water density in Eq. (10), we have:

$$\partial_t \varrho_W = \left(1 + \frac{\varrho_W}{\varrho_S}\right)\nabla_i J_i^W. \tag{56}$$

The above equation relates the rate of change of the partial water density to the water flux through the volume of an infinitesimal representative volume element in space. The last equation could be converted to consider a finite volume V of experimental water retention samples through integration. Using the divergence theorem $\int \nabla_i J_i^W dV = \oint J_i^W dS_i = J_W A$ (having $dS_i = \hat{e}_i dA$, with A being the surface area through which the water flows into V). Therefore, we find that

$$J_W = \left(\frac{\varrho_S}{\varrho_S + \varrho_W}\right)l\partial_t \varrho_W, \tag{57}$$

where $l = \frac{V}{A}$ is the typical experimental dimension. Therefore, the flux of water into the experimental sample scales approximately with the rate of water density and experimental dimension as $J_W \sim l\partial_t \varrho_W$. Using the definitions in Eq. (3), it could also be expressed in terms of rate of the saturation and void ratio:

$$J_W = \mathcal{C}\left(\partial_t S_r + \frac{S_r}{e(1+e)}\partial_t e\right), \quad \mathcal{C} \equiv \mathcal{C}(S_r, e) = l\left(\frac{e}{1+e}\right)\left(\frac{\bar{\varrho}_S \bar{\varrho}_W}{\bar{\varrho}_S + \bar{\varrho}_W S_r e}\right). \tag{58}$$

The above is general. However, in most experimental measurements of soil water retention properties the void ratio e is assumed constant, while the intrinsic densities barely change from their reference:

$$J_W = \mathcal{C}\partial_t S_r \tag{59}$$

359   such that the water flux into the sample relates directly to the rate of saturation.

360   ### 4.8 Non-equilibrium soil water retention

Combining Eqs. (40,44) with Eqs. (48,55), taking as before $\partial_t e \approx 0$ for the experimental conditions, and assuming homogeneous testing conditions for which spatial gradients could be ignored:

$$\partial_t T_m = \frac{\omega R_m}{T_m} = \frac{\omega\gamma(T_{m0}^2 - T_m^2)}{T_m}, \tag{60}$$

where using Eq. (53):

$$T_{\mathrm{m}0} = \sqrt{\tfrac{\eta}{\gamma}} |J_{\mathrm{W}}|, \tag{61}$$

is the stationary solution of T_{m} for $d_t T_{\mathrm{m}} = 0$, which represents the value of the meso-related temperature at the rate independence limit of very slow wetting or drying conditions. The more general case of rate-dependent processes is discussed in Sec. 5.

Next, adopting Eq. (54) along with Eq. (39) for homogeneous testing conditions:

$$\partial_t \xi + r^{\xi\xi} Y_\xi + r^{\xi\mathrm{W}} J_{\mathrm{W}} = 0. \tag{62}$$

When no water is added or subtracted from the experimental sample, where $J_{\mathrm{W}} = 0$, we expect the intrinsic suction deviation ξ to decay towards the true equilibrium only when the meso-scopic interfaces are being sufficiently agitated. Such agitations should expectedly enable to unjam air-water interfaces that may otherwise be pinned in local equilibria along particle roughness and patches of fluids. In the hydrodynamic theory the effects of those agitations on the energy landscape are considered through the meso-related entropy $\jmath_{\mathrm{m}}$ or temperature T_{m}, as conceptualised by Fig. 5. Taking these ideas into account, we require:

$$r^{\xi\xi} = r T_{\mathrm{m}}, \tag{63}$$

with $r \geq 0$, while given the stationary solution of $T_{\mathrm{m}} = T_{\mathrm{m}0}$ in Eq. (61):

$$r^{\xi\xi} = r \sqrt{\tfrac{\eta}{\gamma}} |J_{\mathrm{W}}|. \tag{64}$$

Recalling that $Y_\xi = \kappa\xi$ from Eq. (44), as well as Eq. (59) :

$$\partial_t \xi = -rk\sqrt{\tfrac{\eta}{\gamma}} |J_{\mathrm{W}}|\, \xi - r^{\xi\mathrm{W}} J_{\mathrm{W}}, \quad J_{\mathrm{W}} = \mathcal{C}\partial_t S_r. \tag{65}$$

The above equation represents the main result of this paper – a hydrodynamically resolved equation for soil water retention at non-equilibrium conditions. Accordingly, the intrinsic suction deviation ξ responds hysteretically to cyclical wetting-drying changes to S_r. Notice also that coefficients $\{r, r_{\xi\mathrm{W}}, \eta, \gamma\}$ in Eq. (65) may all depend on the various partial densities ϱ_β, and thus irrespective to cycles the evolution of ξ and thus the non-equilibrium suction would in general depend on those densities (or more specifically on S_r and e). Finally, an even simpler form of this hydrodynamic equation could be developed by noticing that Eq. (65) is entirely rate independent, so material time derivatives in the above equation could be substituted with finite increments (*eg.*, as in $\partial_t x \to dx$):

$$\boxed{d\xi = -\mathcal{A}|dS_r|\xi - \mathcal{B}dS_r} \tag{66}$$

where $\mathcal{A}$ and $\mathcal{B}$ are effective non-negative coefficients for the intrinsic suction deviation, which are given by

$$\mathcal{A} \equiv \mathcal{A}(S_r, e) = rk\sqrt{\tfrac{\eta}{\gamma}}\mathcal{C}, \quad \mathcal{B} \equiv \mathcal{B}(S_r, e) = r^{\xi\mathrm{W}}\mathcal{C}. \tag{67}$$

The above equation for ξ is boxed, as we wish to highlight it as the main result of this paper. While the derivation follows clear yet subtle hydrodynamic concepts, the final result is extremely simple and should thus offer a source of inspiration for future empirical investigations in hydrology and soil mechanics. Given the definition of the non-equilibrium intrinsic suction $\hat{s} = \xi + \hat{s}_{\mathrm{eq}}$ in Eq. (36), a complete model for soil water retention $s = s(S_r, e)$ could then be obtained using Eq. (37), given the relationships for the equilibrium suctions $\hat{s}_{\mathrm{eq}}$ and s_{eq} (here satisfying Eq. (29)).

Since the first term in Eq. (66) linearly scales with ξ, the coefficient $\mathcal{A}$ in it controls the relaxation rate of the system back to equilibrium states. The second term does not depend on ξ and thus the coefficient $\mathcal{B}$ in it controls the drift rate away from the equilibrium state. The actions of these two terms compete, so only if the second term is absent, would the suction deviation relax to zero, thus letting the soil water retention arrive to its equilibrium state. To further understand the role of this competition, consider the stationary case where these terms balance:

$$\xi_{\mathrm{S}} = -\frac{\mathcal{B}}{\mathcal{A}}\frac{dS_r}{|dS_r|} = \mp\frac{\mathcal{B}}{\mathcal{A}} \quad \text{(for } d\xi = 0\text{)}, \tag{68}$$

which does not actually depend on $\mathcal{C}$ and thus on the system dimension l. Considering constant $\mathcal{A}$ and $\mathcal{B}$, once approached ξ remains on its stationary value ξ_{S}. On the other hand, considering $\mathcal{B}/\mathcal{A}$ dependent on S_r and e, the intrinsic suction deviation ξ would drift from ξ_{S}. Nevertheless, the stationary relations in Eq. (68) will be shown to provide a useful indication to the boundaries of the drying and wetting processes. A seemingly robust and simple option for the drift coefficient $\mathcal{B}$ does depend on S_r and e, while the relaxation coefficient $\mathcal{A}$ is kept constant:

$$\mathcal{A} = a, \quad \mathcal{B} = -b\frac{\partial \hat{s}_{\mathrm{eq}}}{\partial S_r}, \tag{69}$$

where $\{a, b\} \geq 0$ are non-negative constants. Since $\hat{s}_{\mathrm{eq}} \equiv \hat{s}_{\mathrm{eq}}(S_r, e)$ may depend on e so does $\mathcal{B}$, and thus the predicted soil water retention curves also vary with e. On the other hand, recall that Eq. (66) ignores the possibility of hysteretic suction due to variable $de \neq 0$, including under constant S_r. Should future experiments explore and report such phenomenon, one may replace the use of J_{W} from Eq. (59) with its more general form in Eq. (58). Note also that under $de = 0$, we find $d\hat{s}_{\mathrm{eq}} = \frac{\partial \hat{s}_{\mathrm{eq}}}{\partial S_r}dS_r$, and so Eq. (66) yields approximately $d\xi = -a|dS_r|\xi + bd\hat{s}_{\mathrm{eq}}$. For $a = 0$ integration gives $\xi \approx b\hat{s}_{\mathrm{eq}}$, showing that the extent of intrinsic suction deviation from its equilibrium would broadly depend on the equilibrium suction level itself. This scaling seems to be universally reflected from experimental retention tests, thus providing the rational basis behind Eq. (69).

4.9 Illustration of non-equilibrium results

Subsection 3.5 illustrates the practical significance of the equilibrium thermodynamic theory by (Jiang et al., 2017) by employing the phenomenological model in Eqs. (33-35). This model allows for a sharper rise of suctions in the vicinity of $S_r = 1$ when compared with their latest phenomenological model in (Einav & Liu, 2020). However, this is not the main result of this paper. The actual aim and result are to clarify the physics of soil water retention in non-equilibrium conditions. For that purpose, here we illustrate this main result by adopting the same equilibrium Eqs. (33-35) as the backbone of the non-equilibrium equations in Eq. (36,38,66). Accordingly, the only two parameters required for capturing non-equilibrium suctions are a and b.

To this end, Fig. 4 presents the effects of these parameters on the non-dimensional intrinsic suction deviation ($\xi^* = \xi/\sqrt{cK_w e^{-\lambda}}$, top row), intrinsic suction ($\hat{s}^* = \hat{s}/\sqrt{cK_w e^{-\lambda}}$, middle row), and measured suction ($s^* = s/(ce^{-\lambda})$, bottom row), for various a and b values. These figures correspond to a suction-controlled protocol, which starts from $S_r = 1$ and $s = 0$, then drying continues till $s^* = 20$, from which we applied 100 small incremental cycles of suction of $\Delta s^* = \mp 2$, followed by further drying till $s^* = 50$, wetting till a negative suction of $s^* = -20$, and final drying back to $s^* = 0$.

Notice that during continuous drainage and imbibition the state is basically roughly parallel to the stationary solutions shown by the dashed orange lines. Furthermore, and most importantly, any deviation from the dashed blue equilibrium curve is attributed to non-equilibrium states. It is shown that in order to regain the equilibrium state one
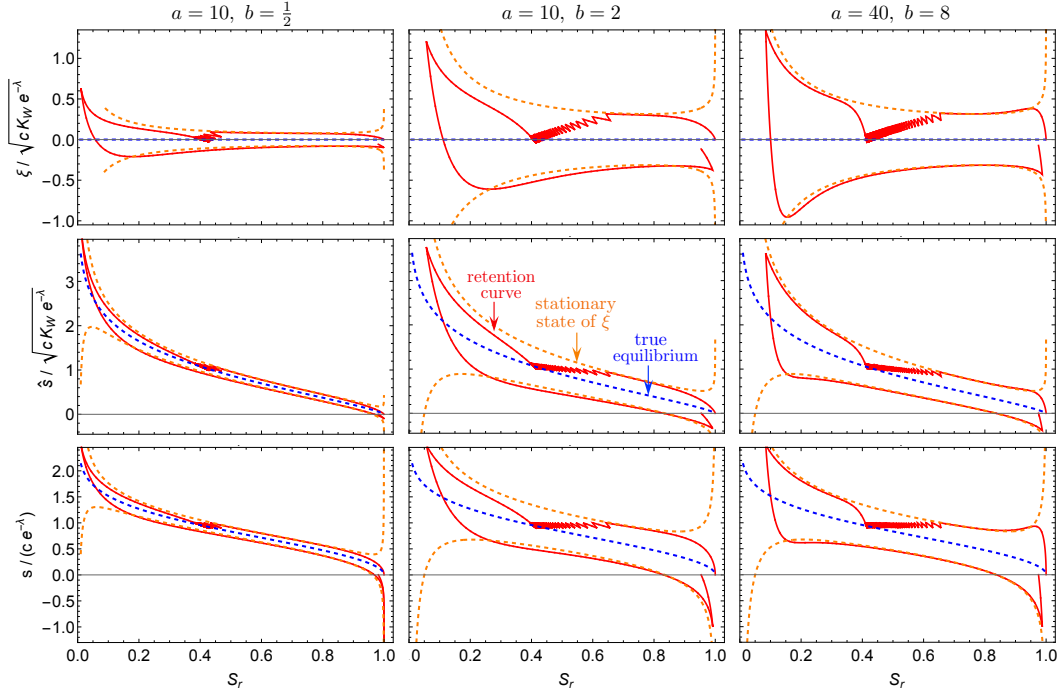
Figure 4: The effects of parameters a and b in Eq. (69) on the dynamics of the intrinsic suction deviation ξ in Eq. (66), the non-equilibrium intrinsic suction $\hat{s}$ using Eq. (36), and the non-equilibrium suction s using Eq. (38), all against saturation S_r. Stationary solutions are given by Eq. (68) and equilibrium states are shown as zero for ξ and using Eqs. (34,33) for the two corresponding suctions.

can add sufficient wetting-drying noise, which causes drifting from the stationary states to the equilibrium one, where $\xi \equiv 0$. For example, ignoring the 100 small cycles, the rest of the curve reveals the previously phenomenologically dubbed (*eg.* see (Alsherif et al., 2015; Beriozkin & Mualem, 2018)): 'first drainage curve' (also known as 'primary drying curve'), 'first imbibition' (also known as 'primary wetting curve') till negative suction, and the following 'secondary drainage' (also known as 'secondary drying curve', as the final leg of our testing protocol, which does not go return to full saturation $S_r <$ 1 at $s = 0$. This inability to regain full saturation after such drying-wetting-drying cycle has been attributed to 'air entrapment' – an obvious synonym for lack of saturation – but we are not aware of clear fundamental explanations to this development besides propositions to use arbitrary curve-fitting protocols. This gap is here filled automatically thanks to the non-equilibrium thermodynamic physics, as we shall further illustrate in the next subsection against experiments.

Finally, it is useful to compare the middle and right columns in Fig. 4, where the a and b coefficients have been quadrupled – this change could arise for example for a given material by quadrupling the experimental dimension l. This is because $\mathcal{C} \sim l$ in Eq. (58), while both $\mathcal{A} \sim a$ and $\mathcal{B} \sim b$ depends linearly on it (Eqs. 68). Since the ratio $\mathcal{B}/\mathcal{A} \sim b/a$ is identical for both columns, the stationary lines on the corresponding figures are identical as well. We thus do not observe much differences when the response follows closely the stationary lines. On the other hand, the rates of approaching to these lines do change significantly, a fact that could be tested experimentally in the future by conducting soil water retention tests for identical materials yet distinctively different sample sizes.

4.10 Metastable states

In Sec. 3.1 the true *equilibrium* conditions involved a previously unspecified list of ζ non-equilibrium internal variables N_ζ. By now this has been addressed, having $N_\zeta \equiv \{\xi, T_{\mathrm{m}}\}$. Being on the minimum energy that corresponds to the true equilibrium the air-water interfaces remain static, and so thus the suction s. Each s-value refers to an S_r-value (and a given e-value). The system is then defined entirely by u_{eq}, from which one can derive the unique equilibrium relationship between suction and densities, as originally derived by (Jiang et al., 2017).

However, in partially saturated soils it is possible to identify other states with motionless fluid-solid interfaces (thus $s_{\mathrm{m}} = T_{\mathrm{m}} \to 0$), which are not under true thermodynamic equilibrium, but rather only *metastable* where the energy landscape is relatively shallow and the stability could be easily perturbed. Under such metastability the non-equilibrium intrinsic suction deviation is not zero $\xi \neq 0$, and thus the energy minimisation is only relative:

$$\min_{\{\hat{\varrho}_\beta, s_{\mathrm{m}}\}} u(s, \varepsilon_{ij}^{\mathrm{e}}, \varrho_\beta, \hat{\varrho}_\beta, \xi, s_{\mathrm{m}}) = u(s, \varepsilon_{ij}^{\mathrm{e}}, \varrho_\beta, \xi) \quad \text{[metastability]} \tag{70}$$

so that unlike Eq. (18) it is found that $u \neq u_{\mathrm{eq}}(s, \varepsilon_{ij}^{\mathrm{e}}, \varrho_\beta)$, because in this case the minimisation does not seek to change ξ. As such, in this case the intrinsic suction deviation from equilibrium is non-zero, so that metastable states do not actually satisfy the thermodynamic equilibrium, even if the system remains static.

To visualise the conceptual difference between the true equilibrium and metastability, it is helpful to schematise the energy landscape using Fig. 5, considering the quadratic non-equilibrium energy in Eq. (43) and the above observations, $s_{\mathrm{m}} \propto T_{\mathrm{m}} \propto |J_{\mathrm{W}}|$.
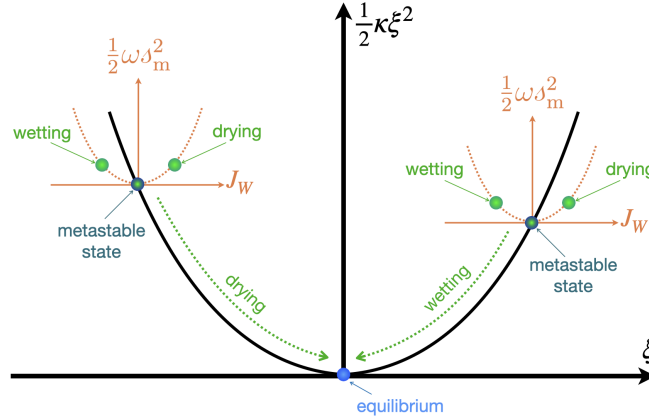

Figure 5: The dynamics of the non-equilibrium energy $u_{\mathrm{ne}} = \frac{1}{2}\kappa\xi^2 + \frac{1}{2}\omega s_{\mathrm{m}}^2$ during wetting ($J_{\mathrm{W}} < 0$) and drying ($J_{\mathrm{W}} > 0$) processes, and the difference between the true thermodynamic equilibrium ($\xi = J_{\mathrm{W}} = 0$) and metastable states ($J_{\mathrm{W}} = 0$).

To clarify further consider pure water or pure air, where each point is in true equilibrium along a plane spanned by the (true thermal) temperature and pressure. There is nothing special here, so one does not need to consider the concept of metastability. On the other hand, dry sand is a classical example for metastability. Here, a sandpile may hold together permanently at a critical angle but any minor perturbation, for example by adding just a single grain, can trigger large parts of it to collapse.

The situation is even more interesting in partially saturated soils, where apart from the intrinsically metastable grains, further complexity arises due to the interaction of the

water with the air through surface tensions, which end up forming feeble fluid patches and interfaces that are only precariously pinned along rough particle surfaces. Here too, any small vibration by gentle shaking, soil shear, or an in- or outward flowing water, can disturb those mesoscopic entities by unpinning interfaces and through the migration, splitting or coalescence of the patches (*e.g.*, see Fig 1b). These dynamics would continue till a new metastable state is met, where the patches stop moving and the interfaces are being pinned along neighbouring roughness points. The meso-related temperature T_{m}, accounting for the random motion of mesoscopic objects such as grains and water-air surfaces, quantifies these motions. The net macroscopic effect of the relaxation of those mesoscopic motions and T_{m} towards zero is seen through the plurality of suction-saturation phenomena, including hysteresis, air entrapment, negative suction and the scanning curves. At any metastable $\{S_r, s, e\}$-point $T_{\mathrm{m}} = 0$. On the other hand, every little noise or perturbation would let T_{m} go up again, thus helping the suction progress to its true equilibrium value – being faster as T_{m} gets larger. Finally, notice that increasing T_{m} through a finite continuous increase of water or air flow, the saturation and void ratio also change, and thus the true equilibrium point is moving as well.

4.11 A mechanical way to departure metastability towards true equilibrium

So far, the derivation focused on pure hydraulic forcing or fluid fluxes along boundaries. Under these conditions it is possible to approach the true equilibrium using small amplitude saturation or suction cycles, as illustrated in Fig. 4. However, there is another approach to explore the new concept of true equilibrium, involving a mechanical source of small amplitude sound waves. To illustrate this point, one can no longer ignore the input of mechanical dissipation $\mathcal{D}$ to the total rate of entropy production in Eq. (47) and thus to the meso-related entropy production R_{m} in Eq. (48). Recalling Eq. (16) that $\mathcal{D} = \sigma_{ij}^{\mathrm{D}}\dot{\varepsilon}_{ij} + \sigma_{ij}^{\mathrm{e}}\dot{\varepsilon}_{ij}^{p}$, the mechanical dissipation may grow from either the development of plastic strain rates ($\dot{\varepsilon}_{ij}^{p}$) or viscous stress ($\sigma_{ij}^{\mathrm{D}}$). Discernible effects from plastic strain rate require sufficient distortion of experimental boundaries. On the other hand, it is possible to generate $\mathcal{D}$ by elevating σ_{ij}^{D} without discernible boundary distortions by viscously heating the meso-scopic structure in the medium using small amplitude sound waves. Accordingly in such experimental configurations the mechanical dissipation could be evaluated from $\mathcal{D} = \sigma_{ij}^{\mathrm{D}}\dot{\varepsilon}_{ij}$. Furthermore, assuming for simplicity that its contribution produce meso-related entropy in R_{m}, the expression in Eq. (48) now becomes

$$R_{\mathrm{m}} = J_i^{\mathrm{W}}\nabla_i X_{\mathrm{Wm}} + \mathcal{D} - \gamma T_{\mathrm{m}}^2, \tag{71}$$

which in the absence of hydraulic fluxes and forcing further simplifies to:

$$R_{\mathrm{m}} = \mathcal{D} - \gamma T_{\mathrm{m}}^2, \quad \mathcal{D} = \sigma_{ij}^{\mathrm{D}}\dot{\varepsilon}_{ij}. \tag{72}$$

This case of the meso-related entropy production is actually equivalent to the original proposition by (Jiang & Liu, 2009) for dry granular media, where the meso-related temperature T_{m} matches the granular temperature. Here, the meso-related temperature cannot be identified as the granular temperature, since it quantifies the motion of all the meso-scopic degrees of freedom of both granular and fluid interfacial entities. Further notice that unlike R_{m} in Eq. (48), whose source term is purely hydraulic, here the source term ($\mathcal{D}$) is purely mechanical and strongly depends on particle motion and viscous heating of the meso-scopic degrees of freedom. This could be understood by noticing that according to the second relation in Eq. (72), to a first order the viscous stress has to be proportional to the strain rate ($\sigma_{ij}^{D} \sim \dot{\varepsilon}_{ij}$) in order to ensure the non-negativity of the mechanical dissipation $\mathcal{D} \sim \dot{\varepsilon}_{ij}\dot{\varepsilon}_{ij} \geq 0$. Exposing an experimental sample to monochromatic sound waves, the meso-related temperature T_{m} would quickly reach a steady state constant value. This occurs when $\dot{T}_{\mathrm{m}} \approx 0$, meaning $R_{\mathrm{m}} \approx 0$, from which $T_{\mathrm{m}} \approx \sqrt{\mathcal{D}/\gamma}$. Having no water flux ($J_{\mathrm{W}} = 0$) into the sample while these waves are being applied, the dissipative flux of the intrinsic suction deviation becomes $Z_\xi = r^{\xi\xi}Y_\xi$ from Eq. (54).

Therefore, using Eqs. (63) and (44) it is possible to write $Z_\xi \sim \sqrt{\mathcal{D}}\xi$, so using Eq. (39) without convection the rate of the non-equilibrium intrinsic suction deviation becomes:

$$\dot{\xi} \sim -\sqrt{\mathcal{D}}\xi. \tag{73}$$

Based on the above result ξ should eventually relax to zero as long as the sound wave continues to produce a non-negative $\mathcal{D} > 0$. Having eventually reached a state with $\xi = 0$ means the true equilibrium of the soil water retention had been reached thanks to non-hydraulic input of external mechanical sound waves.

This new prediction motivates to consider developing novel experiments which incorporate sound waves with which the equilibrium states of soil water retention in a given soil could be discovered and measured systematically. This prediction also vividly highlights the significance of solid mechanics to the comprehensive understanding of soil water retention.

4.12 Comparisons against experimental data

In the absence of clear measurements of intrinsic suction, evaluation against experiments could only be made against previously measured suction-saturation curves (*viz.*, capillary pressure-saturation curves), or suction curves against alternative measures of fluid content. The evaluation below is made under the caveat that rate-dependent effects are mostly not being reported to occur in the experiments, even that those could rather be the rule rather than the exception. To this end, the validity of rate independence is examined in the next Sec. 5, where it is shown that for sufficiently slow loadings, or when there exist long waiting periods between measurement points, where the system can relax to metastable states, the response should indeed represent the limit of rate-independence. Therefore, in this subsection examine the rate-independent limit of the theory where dynamic phenomena are not clearly reported.

In the context of the proposed hydrodynamic theory, unlike previous thermodynamic formulations, rate-independence is not taken as a synonym to true equilibrium. Quite the opposite, hysteresis, air entrapment, and other such phenomena actually reflect non-equilibrium conditions, so rate-independence only relates to metastable states. To illustrate this point, consider the first qualitative comparison of the theory against a previous experiment by (Muraleetharan et al., 2009) in Fig. 6a, which shows the retention response of a finely graded silica sand with a median particle size of 0.14 mm to a comprehensive set of drying-wetting cycles (see more details in (Muraleetharan et al., 2009)). As shown the hydrodynamic model response in Fig. 6b captures the main phenomenological response of this test, including the development of 'air entrapment', the presence of primary and secondary drying and primary wetting curves, and the gradual convergence into a focal point at the end of 'scanning' drying-wetting cycles with diminishing amplitudes. According to the new hydrodynamic theory this focal point resides on the predicted true equilibrium state, as represented by the dashed blue line in Fig. 6b and as explained conceptually using Fig. 5.

It is important to note that the residual saturation in Fig. 6b after the primary drying and wetting back to zero suction does not reside on the true equilibrium line, and so according to our theory the extent of 'air entrapment' that is marked on Fig. 6a should not be seen to be unique, however reproducible it may be during large cycles. To illustrate this point we consider a second comparison, this time against the retention experiment on sintered glass beads by (Poulovassilis, 1970) in Fig. 7. Although the test has been reported to be dynamic, rate-dependent phenomena have not been reported or quantified, and so the prediction is based on the rate-independent limit of the theory. Unlike the previous example, in this experiment the initial drying from full saturation stops at relatively low suction before wetting back to zero suction. Then the extent of drying is increased by achieving a slightly higher suction, to then repeat the wetting back to
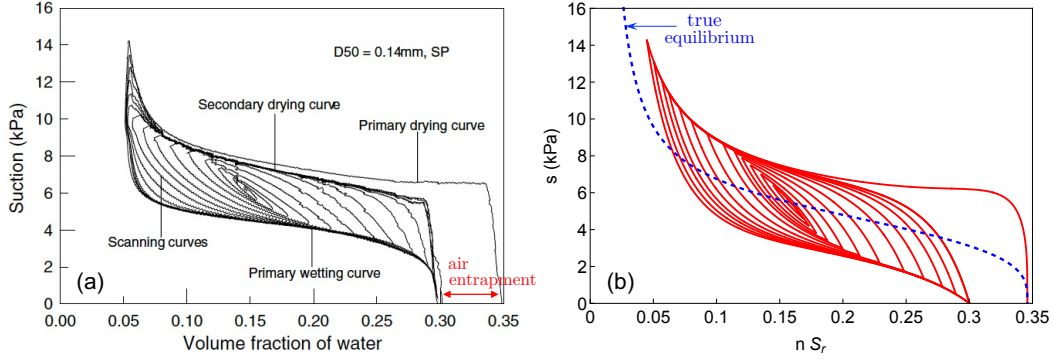
Figure 6: Comprehensive soil water retention under positive suction cycles: (a) experiment by (Muraleetharan et al., 2009), (b) hydrodynamic model response in red with corresponding equilibrium state in dashed blue. Equilibrium parameters: $ce_0^{-\beta} = 5.34$ kPa, $\alpha = 0.3$ and $S_{r0} = 0.015$. Non-equilibrium parameters: $a = 10$ and $b = 2$.

zero suction. Such cycles continue and show that the level of air entrapment is not actually unique, as expected and predicted by the hydrodynamic theory.
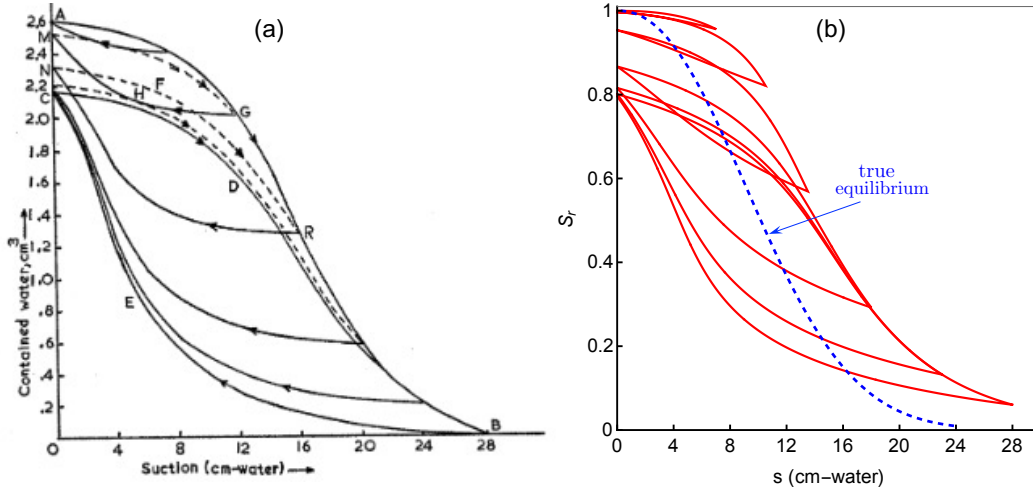

Figure 7: Comprehensive soil water retention under positive suction cycles: (a) experiment by (Poulovassilis, 1970), (b) hydrodynamic model response in red with corresponding equilibrium state in dashed blue. Equilibrium parameters: $ce_0^{-\beta} = 12$ kPa, $\alpha = 0.45$ and $S_{r0} = 0$. Non-equilibrium parameters: $a = 6.8$ and $b = 1.6$.

Notice that in the two previous examples the drying and wetting cycles are made in such a way that the suction always remain positive. Therefore, consider the third comparison in Fig. 8 against experiments on Esperance sand by (Alsherif et al., 2015), who tested the response of soil to wetting-drying cycles in the negative suction domain. Again, the hydrodynamic theory successfully predicts in Fig. 8b the salient phenomenological characteristics of the experimental Fig. 8a. Remarkably, in both cases the small negative suction cycles gradually saturates the sample back towards full saturation. According to the theory, this is because at zero suction the true equilibrium state resides on full

₅₂₄ saturation. Other than using *ad hoc* geometrical algorithms to curve fit such responses,
₅₂₅ we are not aware of any previous first-principle predictions of this phenomenon.
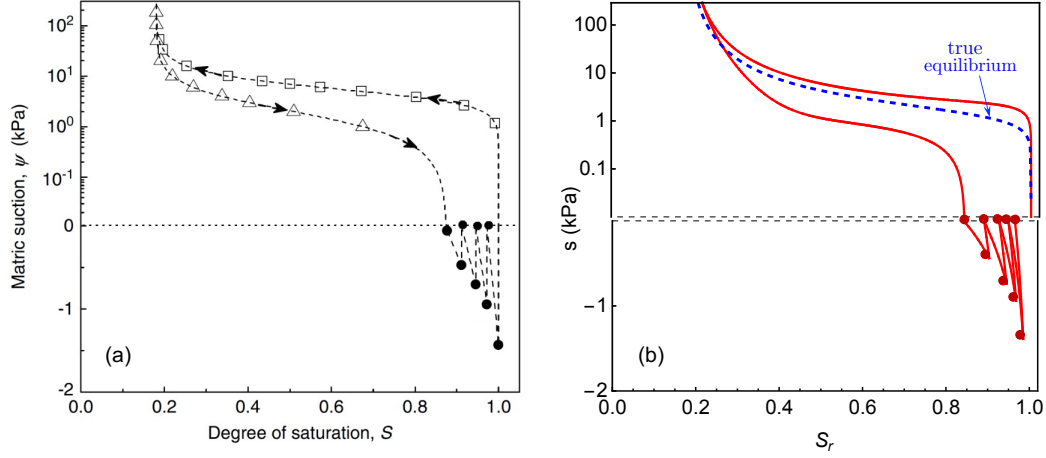

Figure 8: Soil water retention with both positive and negative suction cycles: (a) experiment by (Alsherif et al., 2015), (b) hydrodynamic model response in red with corresponding equilibrium state in dashed blue. Equilibrium parameters: $ce_0^{-\beta} = 1.5$ kPa, $\alpha = 0.35$ and $S_{r0} = 0.18$. Non-equilibrium parameters: $a = 9$ and $b = 1.6$. Points were added for ease of comparison where loading were inverted.

₅₂₆ All the three previous comparisons have been made solely for the soil water reten-
₅₂₇ tion, yet the theory strictly connects this property to the Bishop's effective stress coef-
₅₂₈ ficient χ of partially saturated soil. Where in a previous work (Einav & Liu, 2020) we
₅₂₉ examined this connection against non-cyclical soil water retention experiments for true
₅₃₀ equilibrium conditions, the current theory anticipates the dependence of χ on degree of
₅₃₁ saturation S_r and void ratio e to remain identical for on and off equilibrium conditions.
₅₃₂ To illustrate this point, we consider the final against the experiments of (Khalili & Zargar-
₅₃₃ bashi, 2010) in Fig. 9. While the void ratio e during those tests varied since the sam-
₅₃₄ ples were mechanically loaded to measure χ, the exact variation of e has not been re-
₅₃₅ ported, and thus we keep e constant and equal for both the drying and wetting reten-
₅₃₆ tion curves in Fig. 9a. As such, theoretically speaking under this limit the dependence
₅₃₇ of χ on S_r should remain identical during these legs, as shown in Fig. 9b. This is not
₅₃₈ actually far off from the experimental values reported on that same plot, while the small
₅₃₉ drift during wetting from the drying portion of the χ-S_r relation may be attributed to
₅₄₀ the changes in e during the tests.

₅₄₁ To summarise, the examples above and many similar others we have tried illustrates
₅₄₂ the power of the newly proposed hydrodynamic theory to predict an unprecedented range
₅₄₃ of rate-independent phenomena in partially saturated soils related to soil water reten-
₅₄₄ tion.

5 Non-equilibrium soil water retention (rate-dependence)

₅₄₆ Most common experimental studies of soil water retention attempt to remove po-
₅₄₇ tential rate dependencies at material level. Instead, retention data are recorded only af-
₅₄₈ ter sufficient waiting time, during which the degree of saturation S_r eventually stops chang-
₅₄₉ ing. Excluding macroscopic diffusive flow processes, this observed relaxation may come
₅₅₀ from various dynamic processes such as slow-varying interfacial readjustments, rearrange-
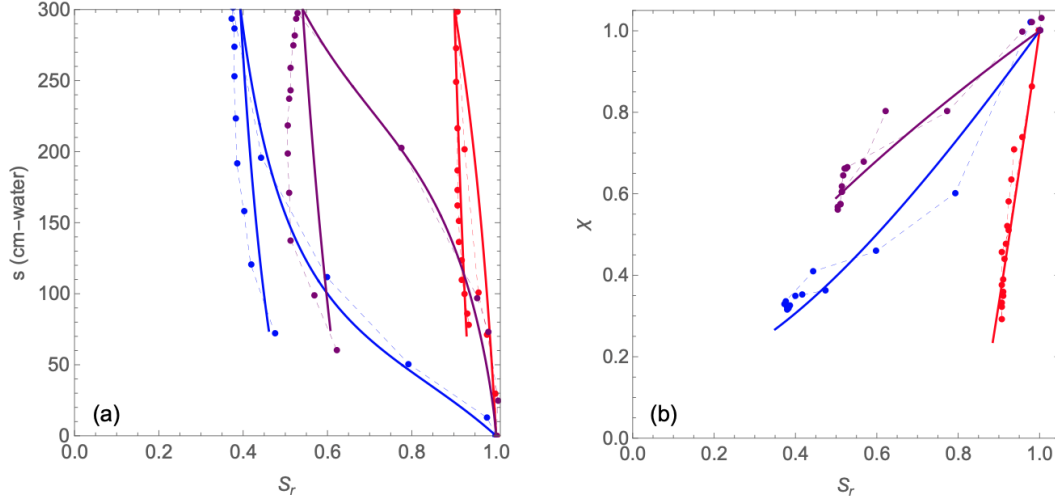
Figure 9: The influence of (a) soil water retention on (b) Bishop's effective stress coefficient. Experimental points come from experiments on three different soils by (Khalili & Zargarbashi, 2010). The solid lines show the hydrodynamic model prediction. For red lines, equilibrium parameters: $ce_0^{-\beta} = 675$ cm-water as a unit of water pressure, $\alpha = 1$, $\lambda = 12$ and $S_{r0} = 0$; non-equilibrium parameters: $a = 18$ and $b = 6.9$. For blue lines, equilibrium parameters: $ce_0^{-\beta} = 7$ cm-water, $\alpha = 0.9$, $\lambda = 0.5$, $S_{r0} = 0.1$; non-equilibrium parameters: $a = 2.5$ and $b = 25$. For purple lines, equilibrium parameters: $ce_0^{-\beta} = 20$ cm-water, $\alpha = 1$, $\lambda = -0.5$ and $S_{r0} = 0.05$; non-equilibrium parameters: $a = 25$ and $b = 140$.

ment of patches of fluids, and diffusion and advection of fluids at the pore-scale. The slow relaxation of S_r during experiments in very short samples, where fluid contents could be considered mostly macroscopically homogeneous, reinforces the possibility that the constitutive process underpinning soil water retention is intrinsically rate dependent. Some experiments actually go beyond to carefully isolate constitutive rate effects from macroscopic flow processes by measuring both saturation and suction at fixed positions in space (Topp et al., 1967; Vachaud et al., 1972; Oung et al., 2005).

The rate dependent effects in these experiments have triggered interest to develop rate-dependent soil water retention models (Hassanizadeh et al., 2002; Helmig et al., 2007). Key features that distinguish the current work from these models is that the current theory automatically captures rate-dependent phenomena thanks to the two-scale temperatures embedded in our hydrodynamic framework. This is on top of the previously discussed differences, including the distinction between true thermodynamic states of equilibrium from metastable states and the measured suction from the intrinsic suction. Specifically, the general rate-dependent evolution equation for the meso-related temperature is simply given by combining Eq. (60) with the stationary meso-related temperature T_{m0} in Eq. (61) to find:

$$\partial_t T_{\mathrm{m}} = \frac{\omega(\eta J_{\mathrm{W}}^2 - \gamma T_{\mathrm{m}}^2)}{T_{\mathrm{m}}}, \quad J_{\mathrm{W}} = \mathcal{C}\partial_t S_r, \tag{74}$$

where the flux J_{W} is a time variable, as it depends on the rate of saturation $\partial_t S_r$ (or more generally, also on the rate of void ratio $\partial_t e$, as specified by Eq. (58)), itself being a time variable. As such T_{m} would not necessarily follow its stationary solution stated in Eq. (61).

Considering a time varying $J_\mathrm{W}(t)$, yet constant $\frac{\eta \varrho_\mathrm{W}}{S_r}$, ω and γ, the above equation could be rearranged

$$\partial_t(\mathcal{L}^2) = \frac{1}{\tau}\left[(\partial_t S_r)^2 - \mathcal{L}^2\right], \quad T_\mathrm{m} = \sqrt{\frac{\eta}{\gamma}}\mathcal{C}\mathcal{L}, \quad \tau = \frac{1}{2\gamma\omega}, \tag{75}$$

where τ is a typical time that controls the relaxation of $\mathcal{L}^2$, while $\mathcal{L}$ acts as a 'memory function' that memorises the time-dependent history of the time-varying saturation rate $(\partial_t S_r)$. Combining the solution of T_m above with Eq. (65), the rate dependent version of Eq. (66) may be rewritten

$$\boxed{\partial_t \xi = -\mathcal{A}\mathcal{L}\xi - \mathcal{B}\partial_t S_r.} \tag{76}$$

which has to be solved in conjunction with Eq. (75). Comparing the above equation with its rate-independent version in Eq. (66) shows that the limit of rate-independence is characterised by:

$$\mathcal{L} \to |\partial_t S_r| \quad \text{(rate-independence)}. \tag{77}$$

The linear differential equation for $\mathcal{L}^2$ in Eq. (75) has a general analytic solution for any time variable $\partial_t S_r(t)$, which can be solved using an integrating factor for the case of initially relaxed $T_\mathrm{m}(t) = 0$, thus giving:

$$\mathcal{L}(t) = e^{-t/(2\tau)}\left(\frac{1}{\tau}\int_0^t e^{t^*/\tau}d_t S_r(t^*)^2 dt^*\right)^{1/2}. \tag{78}$$

It is possible to show that under gradually diminishing $\partial_t S_r(t)$ and slow processes, which develop over times much longer than the typical time $t \gg \tau$, the memory function $\mathcal{L}(t)$ would practically vanish over time, as described by Eq. (77). Therefore, τ simply controls the typical time for the relaxation of T_m to its stationary solution. To illustrate this point, two examples are considered in the section below.

5.1 Monotonic drying from a fully relaxed state

As a first example, consider monotonic drying with constant $\partial_t S_r(t) = -k < 0$ from a state beginning from a fully relaxed state $T_\mathrm{m}(t) = 0$, for which case the integral in Eq. (78) could be resolved to give $\mathcal{L}(t) = \sqrt{1 - e^{-t/\tau}}k$, so that:

$$d_t \xi = -\mathcal{A}\sqrt{1 - e^{-t/\tau}}k\xi + \mathcal{B}k. \tag{79}$$

Therefore, with growing drying time towards $t \gg \tau$ the result practically converges to the rate-independent solution in Eq. (65) for that loading scenario (with $\partial_t S_r = -k$). This dynamic response implied by the theory is demonstrated in Fig. 10 for variously imposed rates of drying. Also demonstrated on that figure is how for (relatively) very low rates of drying k the dynamic response immediately converges to the rate-independent limit response of the theory that is characterised by slow transitions from one metastable state to another.

Also notice from Fig. 10 that the required extent of drying $t{\cdot}d_t\partial S_r$ to return back to equilibrium broadly agrees with $\approx 2\tau{\cdot}\partial_t S_r$, thus given meaning to $\approx 2\tau$ as the typical time above which a drying time $(\partial_t S_r)^{-1}$ would yield the rate independent responses shown in the preceding section.

The above analysis of rate-dependence was done under various imposed saturation rates. This does not directly represent the actual (locally uncontrolled) rates of drying in the previous experiments on rate-dependent effects (Topp et al., 1967; Vachaud et al., 1972; Oung et al., 2005). Nevertheless, the responses observed in Fig. 10 are qualitatively reminiscent to the experimental observations in those studies. In future it could be interesting to pull out the actual rates of drying in those tests, and numerically integrate the equations of $\mathcal{L}^2$.
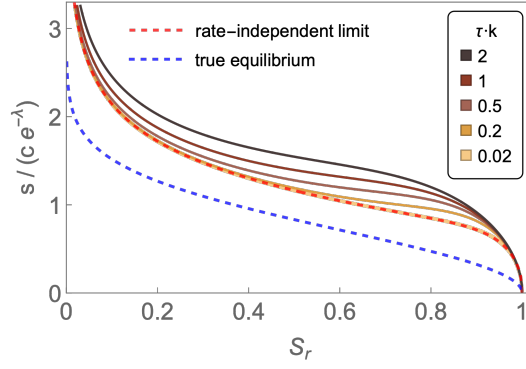
Figure 10: Rate-dependent responses of non-dimensionalised suction-saturation responses under different constant rates of drying $d_t S_r = -k < 0$, starting from full saturation with relaxed state $T_m = 0$. Parameters: $\alpha = 0.5$, $a = 10$ and $b = 2$. Also shown in dashed lines are the rate-independent metastable states and the states corresponding to the true thermodynamic equilibrium. (Attaining the true thermodynamic equilibrium requires perturbations, as described in Sec. 4.)

5.2 Drying-wetting cycles with diminishing amplitude

As a second and slightly more elaborated example consider controlled drying and wetting cycles with diminishing amplitudes from a fully relaxed state $T_m(t) = 0$

$$S_r(t) = 1 - a + a \cos(\pi \tfrac{t}{t_1}) e^{-\tfrac{t}{t_2}}, \text{ for which} \tag{80}$$

$$d_t S_r(t) = -\tfrac{a}{t_1 t_2} \left(t_1 \cos(\pi \tfrac{t}{t_1}) + \pi t_2 \sin(\pi \tfrac{t}{t_1}) \right). \tag{81}$$

where t_1 represents the duration of each drying or wetting leg, and t_2 the typical time during which the drying or wetting amplitudes vanish. A typical example of the variation of S_r with time t is shown on Fig. 11a for the case of $t_2 = 2t_1$, along with its derivative as dashed black line on Fig. 11a.

The form of $\partial_t S_r(t)$ could be integrated analytically using $\mathcal{L}$ in Eq. (78) and yields a closed-form expression. This solution is too long to be illuminating, but its graphical representation is useful and given in Fig. 11b for three different typical times τ. Since the rate independent limit of $\mathcal{L}$ is given by $|\partial_t S_r|$ (see Eq. (77)), it is useful to compare these in Fig. 11b over time. For long varying processes with $\tau \ll t_1$, indeed the rate-dependent response of $\mathcal{L}$ converges to its rate-independent limit. It is then possible to substitute the analytic $\mathcal{L}(t)$ into Eq. (76) and integrate numerically ξ, and then recover the non-equilibrium intrinsic and measured suctions. The corresponding results are shown in Fig. 11c, again highlighting convergence to the rate-independent limit for relatively slow processes.

6 Conclusions

This paper has presented the development of a hydrodynamic theory for partially saturated soils at non-equilibrium conditions. The theory predicts and explains most rigorously and consistently all the pivotal phenomena exhibited by soil water retention relationships. To this end, a number of important theoretical steps have been made that distinguish the current work from previous thermodynamic formulations in the literature.
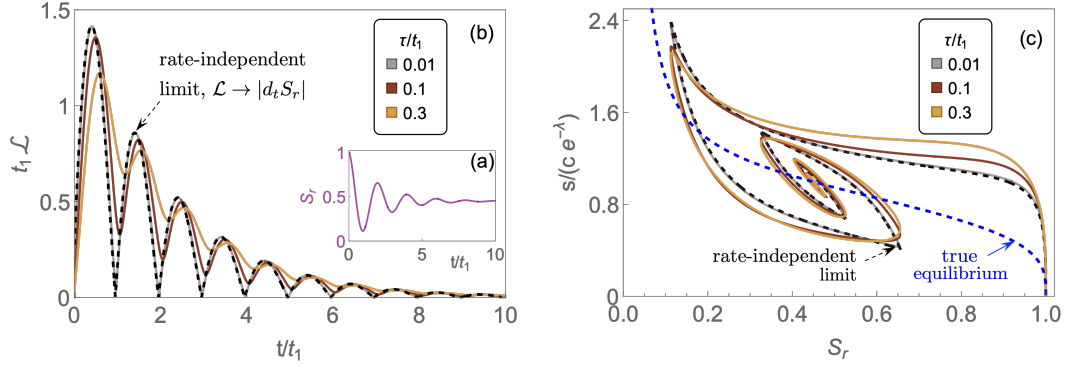
Figure 11: Dynamic drying-wetting cycles with diminishing amplitudes for various typical times τ: (a) saturation over time; (b) memory function over time; and (c) dynamic soil water retention curves.

1. At the limit of thermodynamic equilibrium, the derivation gives results that are fully consistent with the rigorous findings of (Jiang et al., 2017). As such, the derivation carefully distinguished the externally measured/applied suction (or so-called capillary pressure) from the intrinsic suction through chemical potentials in and out the soil, and related these to the effective stress of the soil.

2. To accommodate emergent features at non-equilibrium conditions, the new theory distinguished the true thermodynamic equilibrium from metastable states. It was argued and shown that unlike equilibrium states, metastable states are not unique and can be easily disturbed by external perturbations. Applying such perturbations can lead the system towards its unique equilibrium state.

3. Two non-equilibrium internal variables and their evolution equations were introduced and developed: (a) the intrinsic suction deviation ξ, which simply reflects deviation from the equilibrated intrinsic suction in (Jiang et al., 2017), and (b) the meso-related temperature T_m, which tracks degrees of freedom at the scale of grains and pores.

4. The rate of ξ was rigorously derived based on Onsager's reciprocity principles for dissipative processes at the microscale. The rate of T_m was recovered using the (Jiang & Liu, 2009)'s principle of two-stage irreversibility, which was first proposed to reflect fluctuating grain motions, but here further taken to describe the effects of fluctuating motions of fluid patches and interfaces.

5. At the stationary limit of T_m the new theory predicts rate-independence, where once drying or wetting stop at any given suction-saturation point the system remains metastable. The metastability highlights that these states are rather precarious to small perturbations by wetting-drying cycles or grain agitations.

6. When T_m does not have enough time to relax to its stationary limit, the system shows rate-dependence, as the motion of fluid patches and interfaces means that suction is dynamic.

7. Where the equilibrium and non-equilibrium stationary values of the measured and intrinsic suctions do not depend on experimental sample dimension, the theory reveals that the rate of the approach of the non-equilibrium suction to its stationary value should depend on it.

6.1 Perspectives

6.1.1 Experimental

Apart from explaining previously reported phenomena of soil water retention curves, the proposed theory opens many possible avenues for future research and experiments. For example, a useful experimental contribution could be to further probe the concept of unique equilibrium in partially saturated soils. To this end, one could start applying small amplitude wetting-drying cycles from various degrees of saturation S_r. These cycles could be done as slowly as needed in order to ensure the system travels closely along rate-independent response, visiting only metastable states. Under faster cycles heterogeneities in experimental samples might develop, meaning theoretically a heterogeneous field of meso-related temperature T_m. However, at each point in the domain the true equilibrium retention curve is independent of the magnitude of T_m. A local variation of T_m only modifies the time needed to arrive at this curve, not its form.

A second experimental approach to explore the concept of unique equilibrium would be to apply acoustic waves. Choosing a sound wave that is much larger than the solid particles, neighbouring particles would develop slightly different velocities in them, leading to dissipation of the sound wave, which according to the theory will also increase the meso-related temperature T_m (without even needing to change the saturation S_r). This is quite analogous to viscous heating in water. The smaller the wavelength, the larger are the velocity differences and dissipation. This physics changes when using other forms of waves with a wavelength much smaller than the grains. In this case, if a wave propagates through a grain, the dissipation only heats up the true temperature of this grain, and may not elevate T_m.

Using either of these proposed experimental protocols, whether the initial suction s corresponds to the primary drying or wetting curves, or any other initial state, the final states should end up on a unique relationship between saturation S_r, void ratio e and suction s.

Similarly, the new theory opens new questions on the dependence of the retention of water in a given soil on the dimension of the experimental specimens. The main focus should be on inspecting the slope of the retention curves upon wetting-drying reversals. Furthermore, it followed from the theory that hysteresis in s may also develop at constant S_r yet under cyclical variations in e – developing careful experiments that could impose such conditions could thus be instructive too. Another example for potential experimental exploration would be to study the effect of previous loading rate on metastable states, *e.g.*, according to the theory, the level of suction s should mostly get closer to its equilibrium value s_{eq} while letting it relax after faster drying (or wetting) than slower drying (or wetting).

6.1.2 Theoretical

The proposed theory also opens new questions for further fundamental analyses and developments. For example, while in the current paper the rate-dependent simulations involved controlled saturation rates, these do not actually represent the actual loading conditions in the previous experimental studies (Topp et al., 1967; Vachaud et al., 1972; Oung et al., 2005). Here, neither the rate of saturation nor the suction were actually controlled, but rather measured at local points in space. It is possible to take the measured rate of saturation and integrate along it to study the progression of suction over time. Alternatively, it would be useful to adopt the theory for solving full boundary value problems, involving naturally a hysteretic permeability, thus simulating directly the boundary conditions in these tests, while evaluating the rates of saturation and suction at local points in space and see how they compare with those experiments.

Finally, in this paper the effect of the spatial gradient of the meso-related temperature ∇T_m has been neglected from the entropy production term $F_i^\mathrm{m} \nabla_i T_\mathrm{m}$ in Eq. (45), and as such from the meso-scale entropy balance in Eq. (40). Accounting for it would mean that the rate equation of the meso-related temperature $d_t T_\mathrm{m}$ should further involve a diffusive term $\propto \nabla^2 T_\mathrm{m}$. More specifically, this non-local diffusive term ($\propto \nabla_i^2 T_m$) in the evolution equation for the meso-related temperature (T_m) introduces a diffusive time-scale, which may explain the development of rate-dependent localised patterns within experimental samples, as those are strongly related to the speed of wetting/drying. Capturing such localised features is then possible by treating the experimental sample as a full boundary value problem, with $\nabla_i^2 T_\mathrm{m}$ being evaluated at any point in the experimental domain. An additional diffusive term could be added to the mass conservation of the species in a way that would not violate the overall mass conservation, which would need to be evaluated for any point in the specimen domain. Future research could look deeper into the implication of this term, as it could bring a diffusive length scale to continuum models as it could help them resolving complex patterns in partially saturated media and porous media such as wormholes and fingering (Homsy, 1987; Cueto-Felgueroso & Juanes, 2008).

Considering soil water retention specimens as boundary value problems may also allow capturing additional emerging rate-dependent phenomena, beyond those stated in Sec. 5. For example, each of the mentioned diffusive terms introduces a timescale, in addition to the typical rate-dependence time τ in Eq. 75. Each of these timescales would depend on soil-specific features (*e.g.*, pore and interfacial sizes) and affect measured air entry value and/or hydraulic conductivity. The relative position of the rate of hydraulic loading with respect to any of these material times could inject more quantitative reasoning to why different experimental techniques could be favoured for different materials (*e.g.*, fast imbibition by axis translation for sand, as opposed to drying/wetting through vapour controlled techniques for clay).

Appendix A Parallel flux decomposition of the total entropy production

As mentioned in Sec. 4.5, we considered two possible ways to decompose the $J_i^\mathrm{W} \nabla_i X_\mathrm{W}$ term into R and R_m within the total entropy production $R+R_\mathrm{m}$ of Eq. (47). The formulation in Sec. 4.5 considered a 'parallel force decomposition' of $\nabla_i X_\mathrm{W}$, which was chosen for simplicity. Here, we follow the slightly longer 'parallel flux decomposition' of J_i^W into an atomistic J_i^Wa and meso-related J_i^Wm parts, accordingly:

$$R_\mathrm{m} = J_i^\mathrm{Wm} \nabla_i X_\mathrm{W} - \gamma T_\mathrm{m}^2, \tag{A1}$$

$$R = J_i^\mathrm{Wa} \nabla_i X_\mathrm{W} + Y_\xi Z_\xi + \gamma T_\mathrm{m}^2. \tag{A2}$$

with

$$J_i^\mathrm{Wa} + J_i^\mathrm{Wm} \equiv J_i^\mathrm{W}, \tag{A3}$$

so that by summing R and R_m above, we retain the form of Eq. (47). In other words, in the context of our theory the parallel flux decomposition refers to the way the water flux J_i^W is being decomposed into its atomistic and mesoscopic contributions. In this case, Onsager's reciprocity conditions for the thermal entropy production R are given by

$$\begin{pmatrix} Z_\xi \\ \nabla_i X_\mathrm{W} \end{pmatrix} = \begin{pmatrix} r^{\xi\xi} & r_j^{\xi\mathrm{W}} \\ r_i^{\mathrm{W}\xi} & r_{ij}^{\mathrm{WW}} \end{pmatrix} \cdot \begin{pmatrix} Y_\xi \\ J_j^\mathrm{Wa} \end{pmatrix}, \tag{A4}$$

where the conditions on the generalised resistivity coefficients remain as those stated in Eq. (52). Nevertheless, notice that the meaning of these coefficients changed, and thus their values need not be similar. However, for ease of comparison we do not distinguish the corresponding symbols. Also notice that unlike Eq. (55) in the parallel force formulation, here, in order to ensure $R + R_\mathrm{m} \geq 0$:

$$\nabla_i X_\mathrm{W} = \eta J_i^\mathrm{Wm}. \tag{A5}$$

For convenience, relevant vectors could be represented by their corresponding magnitudes times the unit vector $\hat{e}_i$ along their directions:

$$J_i^{\mathrm{Wa}} = J_{\mathrm{Wa}}\hat{e}_i, \quad J_i^{\mathrm{Wm}} = J_{\mathrm{Wm}}\hat{e}_i, \quad J_i^{\mathrm{W}} = J_{\mathrm{W}}\hat{e}_i. \tag{A6}$$

As before, the stationary solution for the meso-related temperature requires $R_{\mathrm{m}} = 0$, which here means $\gamma T_{\mathrm{m}0}^2 = J_i^{\mathrm{Wm}}\nabla_i X_{\mathrm{W}}$, so that using the above:

$$T_{\mathrm{m}0} = \sqrt{\tfrac{\eta}{\gamma}}|J_{\mathrm{Wm}}|. \tag{A7}$$

Inserting Z_ξ from Eq. (A4) into the evolution equation for ξ in Eq. (39):

$$\partial_t \xi + r^{\xi\xi}Y_\xi + r^{\xi\mathrm{W}}J_{\mathrm{Wa}} = 0, \tag{A8}$$

since $r_i^{\xi\mathrm{W}} = r^{\xi\mathrm{W}}\hat{e}_i$ and $\hat{e}_i\hat{e}_i = 1$.

Similar arguments follow to use Eq. (63), yet the new stationary solution for T_{m} in the form of $T_{\mathrm{m}0}$ in Eq. (A7) above give:

$$r_{\xi\xi} = rT_{\mathrm{m}} = r\sqrt{\tfrac{\eta}{\gamma}}|J_{\mathrm{Wm}}|. \tag{A9}$$

Combining the second Onsager relation in Eq. (A4), the expression for $\nabla_i X_{\mathrm{W}}$ in Eq. (A5), and the one for J_i^{Wm} in Eq. (A3) gives:

$$J_{\mathrm{Wa}} = \frac{\eta J_{\mathrm{W}} + r^{\xi\mathrm{W}}b\xi}{\eta + r_{ij}^{\mathrm{WW}}\delta_{ij}}, \tag{A10}$$

where $\delta_{ij} = \hat{e}_i\hat{e}_j$ is the Kronecker delta. It thus follows that

$$\partial_t \xi = -rb\sqrt{\tfrac{\eta}{\gamma}}\left|J_{\mathrm{W}} - \frac{J_{\mathrm{W}} + \left(\frac{r^{\xi\mathrm{W}}}{\eta}b\right)\xi}{1 + \frac{r_{ij}^{\mathrm{WW}}\delta_{ij}}{\eta}}\right|\xi - r^{\xi\mathrm{W}}\left(\frac{J_{\mathrm{W}} + \left(\frac{r^{\xi\mathrm{W}}}{\eta}b\right)\xi}{1 + \frac{r_{ij}^{\mathrm{WW}}\delta_{ij}}{\eta}}\right). \tag{A11}$$

The above relation serves the same purpose as Eq. (65), which resulted from the parallel force formulation, yet unlike before it is not necessarily rate-independent. However, using the expression for J_{W} in Eq. (59), rate-independence can again be recovered at the limit of $\frac{r_{\xi\mathrm{W}}}{\eta}b \to 0$

$$\partial_t \xi = -rb\sqrt{\tfrac{\eta}{\gamma}}\left(\frac{r_{ij}^{\mathrm{WW}}\delta_{ij}}{r_{ij}^{\mathrm{WW}}\delta_{ij}+\eta}\right)\mathcal{C}\,|\partial_t S_r|\,\xi - r^{\xi\mathrm{W}}\left(\frac{\eta}{r_{ij}^{\mathrm{WW}}\delta_{ij}+\eta}\right)\varrho_{\mathrm{W}}\mathcal{C}\partial_t S_r. \tag{A12}$$

so that we retain the main result of this paper, as boxed in Eq. (66), where instead of Eq. (67), the coefficients in it are now given by

$$\mathcal{A} = rb\sqrt{\tfrac{\eta}{\gamma}}\left(\frac{r_{ij}^{\mathrm{WW}}\delta_{ij}}{r_{ij}^{\mathrm{WW}}\delta_{ij}+\eta}\right)\mathcal{C}, \quad \mathcal{B} = r^{\xi\mathrm{W}}\left(\frac{\eta}{r_{ij}^{\mathrm{WW}}\delta_{ij}+\eta}\right)\mathcal{C}. \tag{A13}$$

Therefore, the parallel flux formulation retains the same evolution equation as boxed in Eq. (66) for rate independent processes. Facing with the same experimental data, the values of the coefficients $\mathcal{A}$ and $\mathcal{B}$ in the evolution equation for ξ would remain similar, yet the values of the Onsager coefficients $\{r, r^{\xi\mathrm{W}}, r_{ij}^{\mathrm{WW}}\}$ may generally be different.

For physical samples, use the IGSN persistent identifier, see the International Geo Sample Numbers section: `https://www.agu.org/Publish-with-AGU/Publish/Author-Resources/Data-and-Software-for-Authors#IGSN`

References

Alaei, E., Marks, B., & Einav, I. (2021). A hydrodynamic-plastic formulation for modelling sand using a minimal set of parameters. *Journal of the Mechanics and Physics of Solids*, *151*, 104388.

Alsherif, N., Wayllace, A., & Lu, N. (2015). Measuring the soil water–retention curve under positive and negative matric suction regimes. *Geotechnical Testing Journal*, *38*(4), 442–451.

Assouline, S. (2006). Modeling the relationship between soil bulk density and the water retention curve. *Vadose Zone Journal*, *5*(2), 554–563.

Bear, J. (2013). *Dynamics of fluids in porous media.* Courier Corporation.

Beliaev, A. Y., & Hassanizadeh, S. M. (2001). A theoretical model of hysteresis and dynamic effects in the capillary relation for two-phase flow in porous media. *Transport in Porous media*, *43*(3), 487–510.

Beriozkin, A., & Mualem, Y. (2018). Comparative analysis of the apparent saturation hysteresis approach and the domain theory of hysteresis in respect of prediction of scanning curves and air entrapment. *Advances in Water Resources*, *115*, 253–263.

Bishop, A. W., & Blight, G. (1963). Some aspects of effective stress in saturated and partly saturated soils. *Geotechnique*, *13*(3), 177–197.

Brooks, R. H. (1965). *Hydraulic properties of porous media.* Colorado State University.

Casimir, H. B. G. (1945). On onsager's principle of microscopic reversibility. *Reviews of Modern Physics*, *17*(2-3), 343.

Chen, P., Lu, N., & Wei, C. (2019). General scanning hysteresis model for soil–water retention curves. *Journal of Geotechnical and Geoenvironmental Engineering*, *145*(12), 04019116.

Cueto-Felgueroso, L., & Juanes, R. (2008). Nonlocal interface dynamics and pattern formation in gravity-driven unsaturated flow through porous media. *Physical Review Letters*, *101*(24), 244504.

de Gennes, P. G., & Prost, J. (1993). *Continuum mechanics.* Clarendon Press, Oxford.

De Groot, S. R., & Mazur, P. (2013). *Non-equilibrium thermodynamics.* Courier Corporation.

Einav, I., & Liu, M. (2018). Hydrodynamic derivation of the work input to fully and partially saturated soils. *Journal of the Mechanics and Physics of Solids*, *110*, 205–217.

Einav, I., & Liu, M. (2020). The effective stress of unsaturated soils: Thermodynamic connections to intrinsic and measured suctions. In *Views on microstructures in granular materials* (pp. 39–60). Springer.

Fredlund, D. G., & Xing, A. (1994). Equations for the soil-water characteristic curve. *Canadian geotechnical journal*, *31*(4), 521–532.

Fukushima, Y., Higo, Y., Matsushima, T., & Otake, Y. (2021). Liquid bridge contribution to shear behavior of unsaturated soil: modeling and application to a micromechanics model. *Acta Geotechnica*, 1–19.

Gallipoli, D. (2012). A hysteretic soil-water retention model accounting for cyclic variations of suction and void ratio. *Geotechnique*, *62*(7), 605–616.

Gallipoli, D., Wheeler, S., & Karstunen, M. (2003). Modelling the variation of degree of saturation in a deformable unsaturated soil. *Géotechnique*, *53*(1), 105–112.

Gan, Y., Maggi, F., Buscarnera, G., & Einav, I. (2013). A particle–water based model for water retention hysteresis. *Géotechnique Letters*, *3*(4), 152–161.

Haines, W. B. (1930). Studies in the physical properties of soil. v. the hysteresis effect in capillary properties, and the modes of moisture distribution associated therewith. *The Journal of Agricultural Science*, *20*(1), 97–116.

Hammervold, W. L., Knutsen, Ø., Iversen, J. E., & Skjæveland, S. M. (1998). Capillary pressure scanning curves by the micropore membrane technique. *Journal of Petroleum Science and Engineering*, *20*(3-4), 253–258.

Hassanizadeh, S. M., Celia, M. A., & Dahle, H. K. (2002). Dynamic effect in the capillary pressure–saturation relationship and its impacts on unsaturated flow. *Vadose Zone Journal*, *1*(1), 38–57.

Hassanizadeh, S. M., & Gray, W. G. (1993). Thermodynamic basis of capillary pressure in porous media. *Water resources research*, *29*(10), 3389–3405.

Helmig, R., Weiss, A., & Wohlmuth, B. I. (2007). Dynamic capillary effects in heterogeneous porous media. *Computational Geosciences*, *11*(3), 261–274.

Homsy, G. M. (1987). Viscous fingering in porous media. *Annual review of fluid mechanics*, *19*(1), 271–311.

Hopmans, J., & Dane, J. (1986). Temperature dependence of soil water retention curves. *Soil Science Society of America Journal*, *50*(3), 562–567.

Jennings, J. E. B., & Burland, J. B. (1962). Limitations to the use of effective stresses in partly saturated soils. *Géotechnique*, *12*(2), 125-144.

Jiang, Y., Einav, I., & Liu, M. (2017). A thermodynamic treatment of partially saturated soils revealing the structure of effective stress. *Journal of the Mechanics and Physics of Solids*, *100*, 131–146.

Jiang, Y., & Liu, M. (2009). Granular solid hydrodynamics. *Granular Matter*, *11*(3), 139.

Jiang, Y., & Liu, M. (2015). Applying GSH to a wide range of experiments in granular media. *The European Physical Journal E*, *38*(3), 1–27.

Kamrin, K., & Bouchbinder, E. (2014). Two-temperature continuum thermomechanics of deforming amorphous solids. *Journal of the Mechanics and Physics of Solids*, *73*, 269–288.

Khalatnikov, I. M. (2018). *An introduction to the theory of superfluidity*. CRC Press.

Khalili, N., & Zargarbashi, S. (2010). Influence of hydraulic hysteresis on effective stress in unsaturated soils. *Géotechnique*, *60*(9), 729–734.

Landau, L. D., & Lifshitz, E. M. (1980). *Statistical physics*. Butterworth-Heinemann.

Landau, L. D., & Lifshitz, E. M. (1987). *Fluid mechanics*. Butterworth.

Li, S. X., Pengra, D. B., & Wong, P.-z. (1995). Onsager's reciprocal relation and the hydraulic permeability of porous media. *Physical Review E*, *51*(6), 5748.

Liu, M. (2021). Temperatures in grains and plasma. *EPL (Europhysics Letters)*, *135*(3), 36003.

Morrow, N. R. (1970). Physics and thermodynamics of capillary action in porous media. *Industrial & Engineering Chemistry*, *62*(6), 32–56.

Moyne, C., & Murad, M. A. (2006). A two-scale model for coupled electro-chemo-mechanical phenomena and onsager's reciprocity relations in expansive clays: I homogenization analysis. *Transport in porous media*, *62*(3), 333–380.

Mualem, Y. (1976). A new model for predicting the hydraulic conductivity of unsaturated porous media. *Water resources research*, *12*(3), 513–522.

Muraleetharan, K. K., Liu, C., Wei, C., Kibbey, T. C., & Chen, L. (2009). An elastoplastic framework for coupling hydraulic and mechanical behavior of unsaturated soils. *International Journal of Plasticity*, *25*(3), 473–490.

Onsager, L. (1931). Reciprocal relations in irreversible processes. i. *Physical review*, *37*(4), 405.

Oung, O., Hassanizadeh, S. M., & Bezuijen, A. (2005). Two-phase flow experiments in a geocentrifuge and the significance of dynamic capillary pressure effect. *Journal of Porous Media*, *8*(3).

Pasha, A. Y., Khoshghalb, A., & Khalili, N. (2017). Hysteretic model for the evolution of water retention curve with void ratio. *Journal of Engineering Mechanics*, *143*(7), 04017030.

Poulovassilis, A. (1970). The effect of the entrapped air on the hysteresis curves of a porous body and on its hydraulic conductivity. *Soil Science*, *109*(3), 154–162.

Rubin, M. B., & Einav, I. (2011). A large deformation breakage model of granular materials including porosity and inelastic distortional deformation rate. *International Journal of Engineering Science*, *49*(10), 1151–1169.

Skjaeveland, S., Siqveland, L., Kjosavik, A., Thomas, W., & Virnovsky, G. (2000). Capillary pressure correlation for mixed-wet reservoirs. *SPE Reservoir Evaluation & Engineering*, *3*(01), 60–67.

Topp, G., Klute, A., & Peters, D. (1967). Comparison of water content-pressure head data obtained by equilibrium, steady-state, and unsteady-state methods. *Soil Science Society of America Journal*, *31*(3), 312–314.

Vachaud, G., Vauclin, M., & Wakil, M. (1972). A study of the uniqueness of the soil moisture characteristic during desorption by vertical drainage. *Soil Science Society of America Journal*, *36*(3), 531–532.

Vaunat, J., & Casini, F. (2017). A procedure for the direct determination of bishop's χ parameter from changes in pore size distribution. *Géotechnique*, *67*(7), 631–636.

Viggiani, G., & Atkinson, J. (1995). Interpretation of bender element tests. *Geotechnique*, *45*(1), 149–154.

Wang, S., Tokunaga, T. K., Wan, J., Dong, W., & Kim, Y. (2016). Capillary pressure-saturation relations in quartz and carbonate sands: Limitations for correlating capillary and wettability influences on air, oil, and supercritical co2 trapping. *Water Resources Research*, *52*(8), 6671–6690.

Wardlaw, N. C., & Taylor, R. (1976). Mercury capillary pressure curves and the intepretation of pore structure and capillary behaviour in reservoir rocks. *Bulletin of Canadian Petroleum Geology*, *24*(2), 225–262.

Winkler, M., Gjennestad, M. A., Bedeaux, D., Kjelstrup, S., Cabriolu, R., & Hansen, A. (2020). Onsager-symmetry obeyed in athermal mesoscopic systems: Two-phase flow in porous media. *Frontiers in Physics*, *8*, 60.

Zhao, B., MacMinn, C. W., Szulczewski, M. L., Neufeld, J. A., Huppert, H. E., & Juanes, R. (2013). Interface pinning of immiscible gravity-exchange flows in porous media. *Physical Review E*, *87*(2), 023015.

Zhou, A.-N. (2013). A contact angle-dependent hysteresis model for soil–water retention behaviour. *Computers and Geotechnics*, *49*, 36–42.

Zhou, A.-N., Sheng, D., & Carter, J. P. (2012). Modelling the effect of initial density on soil-water characteristic curves. *Géotechnique*, *62*(8), 669–680.